# DEVELOPMENT OF THE CALIBRATION SCHEME AND SYSTEM INTEGRATION OF THE ÖZYEĞIN BIOPSY ROBOT (OBR)

A Thesis

by

Mirza Awais Ahmad

Submitted to the
Graduate School of Sciences and Engineering
In Partial Fulfillment of the Requirements for
the Degree of

Master of Science

in the
Department of Electrical and Electronics Engineering

Özyeğin University
August 2016

# DEVELOPMENT OF THE CALIBRATION SCHEME AND SYSTEM INTEGRATION OF THE ÖZYEĞIN BIOPSY ROBOT (OBR)

Approved by:

Assist. Professor Özkan Bebek, Advisor
Department of Mechanical Engineering
*Özyeğin University*

Assist. Professor Cenk Demiroğlu
Department of Electrical and Electronics Engineering
*Özyeğin University*

Assoc. Professor Duygun Erol Barkana
Department of Electrical and Electronics Engineering
*Yeditepe University*

Date Approved: 16 August 2016

*To the two pillars of my life, Allah and my Parents.*

# ABSTRACT

Imaging systems can fail to visualize cancerous tissues for proper diagnosis. Needle based procedures, like biopsies, increase the chances of accurate diagnosis of tumors. These procedures also have applications in minimally invasive treatments and regional anesthesia. In recent years, robotic systems have found their way into medical applications of needle based interventions by increasing the accuracy of these procedures. Precise needle positioning is critical in such medical applications.

This thesis presents the architecture of a robotic system designed for human biopsies. The system includes a 5 DoF parallel robot that can be used in Ultrasound (US) guided percutaneous needle interventions. US imaging is used as the visual feedback. The imaging system must be calibrated in 3D space before integrated with the biopsy robot. A novel method for 3D space calibration using a multipoint cross-wire phantom is introduced in this dissertation. The calibration process is improved using wires parallel to the US image plane in order to locate the exact image position in 3D space. Most of the methods fail to consider the errors caused by this intrinsic assumption that the plane exists at the midpoint of the US probes base, while probe holding fixtures can cause minute offsets leading to positional inaccuracies. The final calibration experiments resulted in accuracy of 0.03 mm RMS error.

Details of real time functionality of the robotic system components working with spatial and computational synchronization is also presented. The real-time operation enables the robotic system to perform autonomously. This ability is demonstrated by tracking a moving target with the needle tip motion with an RMS error of 0.23 mm.

# ÖZETÇE

Görüntüleme sistemleri doğru tanı için kanserli dokuları görselleştirmekte başarısız olabilirler. Biyopsi gibi iğne tabanlı işlemler, tümörlerin doğru tanı olasılığını artırmak için kullanılmaktadır. Bu işlemler arasında minimal girişimsel tedaviler ve bölgesel anestezi uygulamaları da vardır. Son yıllarda, robotik sistemler bu prosedürlerin doğruluğunu artırarak iğne temelli müdahalelerin tıbbi uygulamalarda kullanılması arttırmıştır. İğnenin Hassas konumlandırması tıbbi uygulamalarda başarı için önemlidir.

Bu tez, insan biyopsisi için tasarlanmış bir robot sisteminin yapısını açıklamaktadır. Sistem Ultrason (US) destekli perkütan iğne müdahalelerinde kullanılan bir 5 serbestliğe sahip paralel robot kapsamaktadır. US görüntüsü görsel dönüt olarak kullanılmaktadır. Görüntüleme sisteminin biyopsi robotu ile entegre edilmesinden önce 3 boyutlu (3B) uzayda kalibre edilmesi gerekmektedir. Çoklu çapraz-tel fantom kullanarak 3B uzayda kalibrasyon için yeni bir yöntem bu tezde anlatılmaktadır. Kalibrasyon işleminde tellerin 3B alanda konumunu bulmak için US görüntü düzlemine paralel teller kullanıldı. Diğer yöntemlerin çoğunluğu sondayı tutan fikstür ile oluşan konumsal hatayı ve US görüntü düzleminin sonda tabanının ortasında varsayılmasıyla oluşan hataları yok saymaktadır. Nihai kalibrasyon deneyleri 0.03 mm etkin değer hata doğruluğu ile sonuçlanmıştır.

Konumsal ve zamansal senkronizasyonu yapılmış bileşenler ile çalışan robotik sistemin gerçek zamanlı işlevselliğinin detayları da sunulmaktadır. Gerçek zamanlı denetim, robotun özerk sistem olarak çalışmasını sağlamaktadır. Bu kabiliyet, hareketli iğne ucunu 0.23 mm'lik etkin değer hata ile takip edilerek gösterilmiştir.

# ACKNOWLEDGEMENTS

I will take this opportunity to thank my adviser Dr. Özkan Bebek for accepting me as his Masters student. I found working with him very pleasant because of his kind, considerate and positive personality. He always kept me motivated for the research through his guidance and encouragement during my research. He set realistic goals and deadlines and trusted me, which gave me the confidence to perform efficiently to my best efforts. I have learnt a lot from him and I am grateful for his encouragement, support, and patience which enabled me to complete this thesis.

I would also like to thank Dr. Barkan Ugurlu and Dr. Erhan Öztop for their support and sharing their knowledge which helped me improve my research. My thanks also go to the other members of thesis defense committee, Dr. Cenk Demiroğlu and Dr. Duygun Erol Barkana, for contributing towards finalizing my work with their precious and positive feedback.

I owe a lot of thanks to my colleagues at the Özyeğin Robotics Lab. They made my time at this lab enjoyable by their friendship, and made me work harder by their support and inspiration. We shared a lot of time at the lab studying for courses and working together days and nights. I would also like to thank my friends outside the lab for making living without family easier.

Special thanks to my family for their endless love and encouragement. They gave me the opportunities of education from the best institutions and provided unconditional support, both financially and emotionally throughout my life.

This research was done in the Robotics Laboratory at Özyeğin University; supported by the Scientific and Technical Research Council of Turkey (TUBITAK) under Grant No. 112E312.

# TABLE OF CONTENTS

# LIST OF TABLES

## LIST OF FIGURES

# CHAPTER I

# INTRODUCTION

Needle biopsies are performed to collect tissue samples from the patients body for analyses and diagnoses. Biopsies can be used to take samples from a patients muscles, bones and organs like liver and prostrate. According to American Cancer Society, Breast cancer is the leading diagnosed cancer in women and second most fatal. Also prostrate cancer among men is the second most commonly diagnosed cancer [1]. Imaging technologies like Ultrasound are the primary method to detect tumors but they provide very little information about the type or stage of cancer that's why sometimes needle biopsies are suggested. Physicians and surgeons have to be careful while taking out samples, as wrong samples can lead to wrong diagnosis. In order to be sure, physicians normally take multiple samples, which are painful for the patients and can create post-procedure complications by damaging the healthy tissue. Recent developments in the robotic technologies have given the courage to introduce robotic systems in medicine. In percutaneous operations, robotic systems have provided valuable improvements in the outcomes. They provide high precision and consistency in these complex operations.

In the recent years, many autonomous and tele-operated mechanisms have been developed for needle operations. These autonomous systems contain an imaging system for visual feedback and an instrument manipulator robot. Some commonly used imaging systems are Computed Tomography (CT), Magnetic Resonance (MR) [2], and Ultrasound (US) technologies. The outputs of these imaging systems are used to track both the target tissue and the surgical instrument in patients body. Derived information from the images is a feedback for the robotic manipulator and helps the needle to reach its target. On the other hand, in manual operations, the robots help the surgeons to maintain motion stability in long and tiring operations, and even surgeons can perform these operations from a remote location.

In the literature, custom robotic systems have been developed for specific tissues like brain[3], breast[4, 5], kidney [6], lung [7] and prostrate [8, 9] . In addition, there are systems developed for small animals[10, 11, 12, 13] for medical studies. Common design purpose of these systems is to reduce the human error and to get the required accuracy and reliability in the process. A few examples of such systems are given. Chung *et al.* [10] developed a 4-DOF mechanism with a five-chain system, Goffin *et al.* [11] developed a 6-DOF mechanism for small animal biopsies. The mechanism used a $\mu$CT imager and a stereo camera. While the stereo camera was used for positioning, $\mu$CT images were used for in vivo targeting of the small animals tissue. Huang [12] developed a biopsy robot for small animals in which the design of the robot is compatible with MR imaging. In the system the syringe is held by a CASTPRO-II robotic arm. Due to the highly accurate robotic arm, the positioning accuracy of the system was 0.05$\pm$ 0.39 mm (mean$\pm$deviation).

Yang [5] built a pneumatically actuated 4 DOF parallel mechanism robot for breast biopsies. Yangs system uses MR imaging to target the tissue. Biopsies were performed by the earlier mechanisms designed in the literature, however, Tanaiutchawoot *et al.* [4] designed a passive mechanism which holds and helps the needle positioning by using tissue attributes for breast biopsies. The 5 DOF system uses a real-time vision based system with markes for positioning. Moon [7] developed a compliant mechanism in order to correct the needle axis during needle interventions. Also, Moon *et al.* [14] designed a second mechanism for the cases where the needle bends due to the skin stiffness.

Needle interventions have also found their applications in areas other than biopsies. They are also being used as treatments and drug delivery mechanisms. Morse *et al.* [15] have discussed the use of needle intervention as a mean to induce regional anesthesia using nerve blocking. They have also compared the performance of manual vs. robot assisted operation. Needle interventions are also being used as a treatment technique called cryosurgery or also known as cryoablation [16, 17, 18]. In this technique, liquid nitrogen is injected around the cancer affected cells to kill them by freezing.

During the past few years, Minimally Invasive Surgery (MIS) has also found its way to popularity among surgical techniques due to the reduced post-surgical recovery time. In general, MIS procedures require high accuracy due to the restricted end effector workspace, hence robots are designed to assist in MIS. Kettenbach *et al.* [19] also built a biopsy system for MIS. The biopsy robot was tested on gel phantoms that integrate peas to mimic tumors in tissues.

Among the available imaging techniques, 2D-US imaging devices cost lower than the other options. A disadvantage of US imaging is its excessive artifacts and low resolution, which makes needle tip tracking and detection challenging [20]. Kaya and Bebek [20, 21] proposed a method to detect the needle axis and its tip based on the Gabor filtering. The proposed method highlights the needle in the US image while suppressing artifacts. The algorithm estimates the needle insertion angle, and detects the needle's tip in real-time.

Özyeğin Biopsy Robot is designed to perform in vivo needle biopsies. OBR is a 5 DOF-robotic system and uses US imaging to detect needles and target tissue. OBR is designed for multi-purpose biopsy procedures, mostly focusing on the abdominal region. A target position is given by detecting an anomaly using US device. The robot can position itself with the desired attitude and the needle insertion is performed by the robot autonomously. Using a different end effector tool, drug delivery procedures could also be applied.

## *1.1 Thesis Contribution*

The work done during this thesis dissertation have led towards the development of Özyeğin Biopsy Robot, which is a complete robotic biopsy system. This work bridges the work done by Orhan *et al.* in [22] and Kaya *et al.* in [20, 21, 23, 24] to make the real time autonomous robotic biopsy possible.

The initial work done was published in 17th International Conference on Advanced Robotics 2015. It presents the calibration scheme of 2D US images in 3D space for robotic biopsies proposed at an earlier stage [25]. Later improvements have led to the creation of a novel technique for the calibration process. The work done about the System Integration and Target Tracking concludes the project with promised results.

## *1.2 Thesis Outline*

This thesis is organized as follows. Chapter I is the basic introduction of the problem. Chapter II discusses the calibration scheme for the 2D US images with relevant literature. Chapter III talks about the system components and their integration in the system architecture for real time operation. Chapter IV is about the controller design for motion tracking of a target with the biopsy needle. Chapter V presents the research done on the compliant motion of a robotic arms and uses the pre-built force-control function of an industrial robot to achieve compliant motion of US probe. Finally, Chapter VI discusses the conclusion.

# CHAPTER II

# CALIBRATION SCHEME

The purpose of the biopsy robot is to reach a target tissue, using Ultrasound image as visual feedback. A calibration scheme is needed because the biopsy robot has its own coordinate frame of reference but the information about the target point exists inside US image. The calibration process gives a transformation to correlate these two coordinate frames with respect to each other. In this chapter, the crosswire multi-thread method for the calibration of US images is presented.

## *2.1 Previous Work in Literature*

Ultrasound is a noninvasive imaging technology. While there are other noninvasive technologies as well, like X-rays and MRI, but US is safer and cheaper to use. US machines are also smaller and portable hence easy to use and long exposure to US is not dangerous for the patients. US is capable of imaging tissues and organs in real time. Smith et. al. in [26] explains the use of US for lesion excision in breast biopsies and Rifkin et. al. in [27] reports some results of using 2D-US imaging in liver biopsies. Both conclude the usefulness of US imaging at the clinical setting. In many clinic cases, US can bring innovative and effective solutions for the procedures.

2D US has its own limitations. It is difficult for a physician to understand the form of a tissue just from a single 2D US image [28]. That's why most of the time physicians sweep the 2D-probe over the area or rotate around the area to get a 3D sense of the tissue. Hence, 3D US probes have been developed to remedy this problem. In 3D US machines anatomical structures are directly visualized in 3D volume which improves diagnostics and decision making. 3D US images can be used to examine a developing fetus, the brain motion during neurosurgical operations, or to detect the size of a tumor [29]. Robotic systems have also been introduced in medicine to perform US imaging on patients due to their precision and repeatable dexterity [30].

Mercier et. al. in [31] have discussed four main methods which can realize 3D US images. One of the methods is to use 3D probes that are already in the market. These probes work on the same principle as 2D probes but instead of having a single array of US sensors, they contain multiple arrays of sensors taking images simultaneously. Normally these arrays are spread in radially conical form on the tip, and due to small space available for the sensors, the resolution is low. In other type of probes, a single array of sensors is moved inside the probe tip to scan the area and construct a 3D volume. Radial movement of the sensor array increases the field of view. These probes are relatively larger and expensive.

Another way to achieve US volume is to traverse US probe using a motorized mechanism. The US probe is moved through a 3D space taking images on regular intervals and on a predefined path and a US volume is created using these image slices. The probe can be moved in linear path where parallel planes are captured from the 3D space [1], or radial paths [32] in which the probe is rotated around a pivot forming a cylindrical 3D US volume. The method is not complicated but it may result with less accurate information due to constrained motion of the probe. Usually the probe is tracked using a motion sensing technique. Some studies also report sensorless calibration estimation by applying speckle regression to the US images.[33].

In this thesis the freehand calibration technique is used in which the motion of the probe is not constrained. The data of the position and the orientation of the probe in 3D space is collected using a motion capture system, which helps determine the location of the imaging plane and its pixels with respect to the biopsy robot. The motion of the probe is tracked using either optical type, mechanical contact type, or magnetic tracking sensors. The freehand calibration technique's effectiveness depends on the motion of the probe; however it provides the flexibility of the 3D US probes while having no limits on the trackable volume. If the calibration volume is covered fully with smooth movement of the probe, calibration space will be homogeneous. Eirik *et al.* [34] have used the freehand technique to calibrate the US images using an optical tracking system and a sphere of pre-known dimensions.

This thesis presents calibration using a crosswire multithread phantom. The calibration phantom design went through two phases. In first phase, the cross wires in the setup were only in the perpendicular direction of the US image plane which compromises the accuracy of the measurements in the plane parallel to US image. In the second phase, the design of the phantom was improved and new threads are introduced parallel to the US image plane. The effects of these parallel threads on the accuracy of the calibration process are discussed in the following section. This calibration process combined with the needle tracking in US images is used to bring the biopsy robot and the moving needle tip to the same universal coordinate system, allowing the robot to accurately perform the biopsies. The contribution of the work done by Kaya *et al.* [24] on needle tracking in US images is discussed in Chapter IV.

## 2.2 Construction of the Calibration Phantom

The phantoms used in this study are US compatible coupling materials. Phantom design is important in calibration process, as we embed objects of known shapes and dimensions in them and collect US images. Typically phantom is a tissue like soft material, i.e., gel, silicon, agar or combination of them or it can simply be water. Objects with known attributes can be embedded to the test phantoms. These geometries can be simple threads or wires passing through the phantom matter; or objects of known dimensions [35]. In our setup, threads are used in a water tank to make the calibration phantom.

As stated earlier, the calibration tank went through two design phases. The first design had 8 threads as the cross-wires which cross the US image plane at an angle.

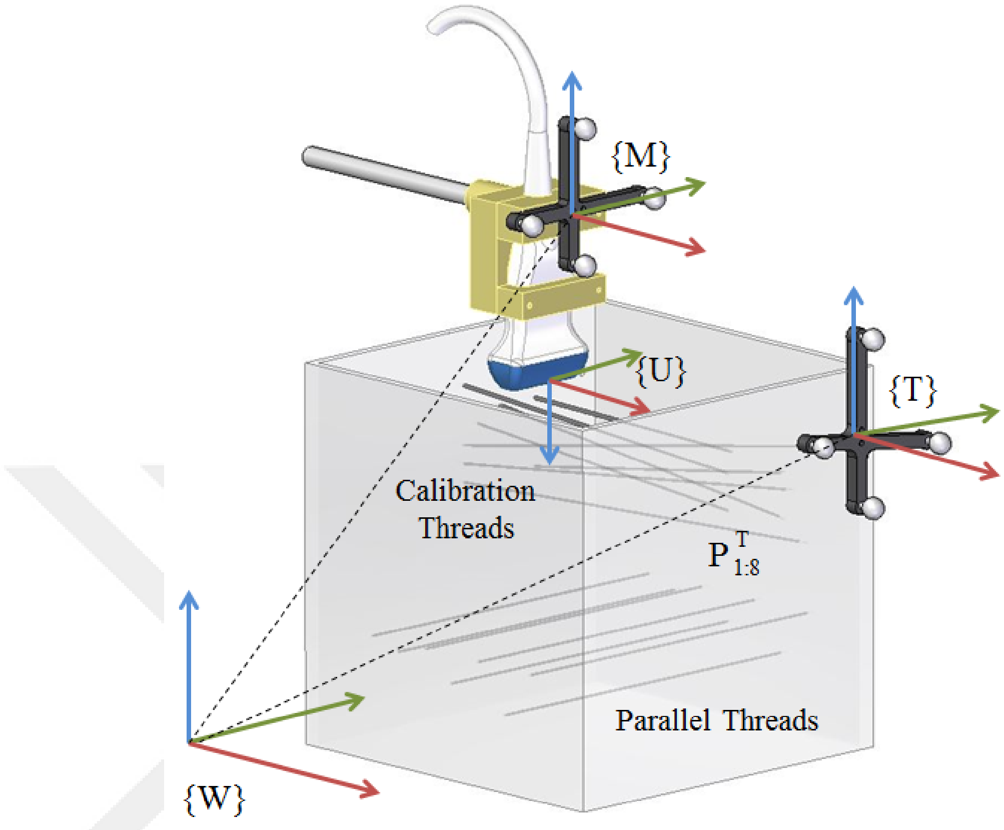


**Figure 1:** Calibration block diagram with marker frames on the US probe {M}, Calibration Tank {T}, US image plane {U} and the crosswires $P^T$

These cross-wire threads originate from one wall of the calibration tank and end at the opposite wall. A frame of reference is assumed to provide reference to the location of the threads with respect to the calibration tank. In reality this frame of reference belongs to the optical marker attached to the calibration tank as shown in Fig. 1.

For calibrating the US image using the cross-wires, the actual cross-sectional position of the threads at any distance must be known. This location can be found by a mathematical model as these threads can be represented by lines connecting two points of known coordinates. This mathematical model of the calibration box is made in Matlab. In this Matlab model, a virtual image plane is generated which exists inside the tank. The locations where this plane intersects with each cross-wire can be found. Fig. 2 shows the mathematical model of the calibration tank with the cross-wires and the virtual US image plane. This model gives the location of each thread inside the image frame in millimeters.

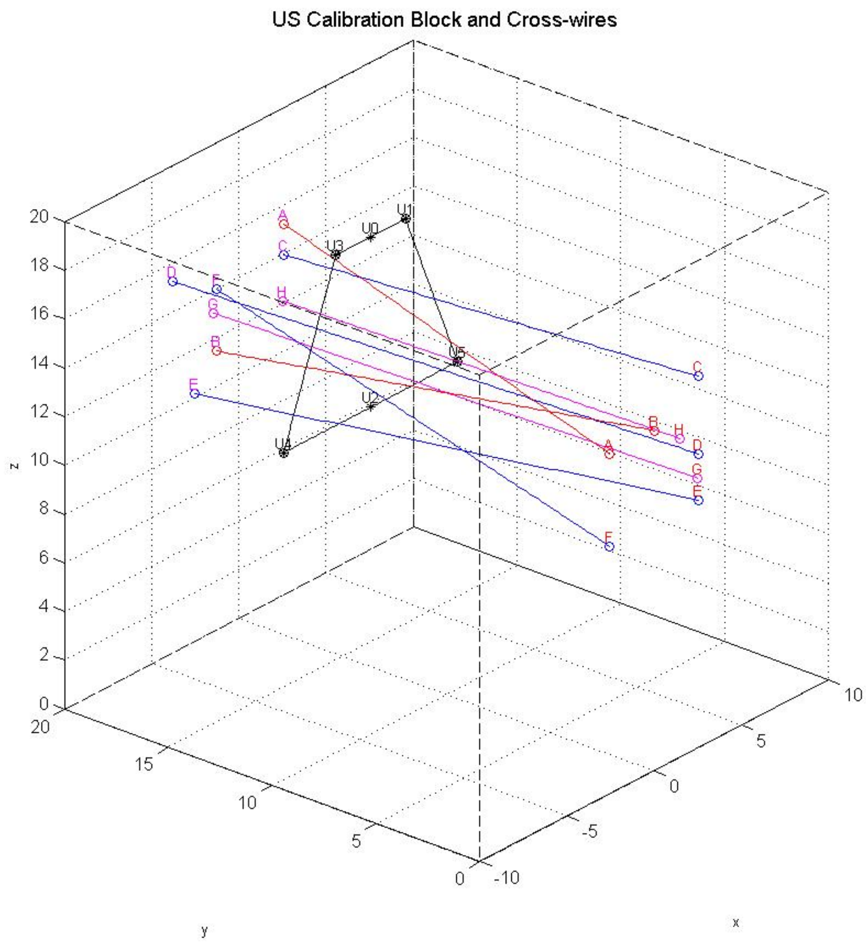


**Figure 2:** Model of the calibration box with 8 cross-wire threads

To find the solution of the calibration problem, an actual US image is compared with the mathematical model. The exact position and orientation of the US probe inside the tank is tracked by a motion tracking system and then sent to the mathematical model of the tank. This model returns the locations of the threads at the given position and orientation of the US prob. This information is used to calibrate the corresponding US image which has the thread locations in the units of pixels. This calibration is the scaling factors to convert units of pixels to millimeters.

Above mentioned calibration technique is prone to some errors due to the assumption that exact location of the US image plane in 3D space is known. In reality it is not true. The knowledge of the exact location of the image plane is very crucial to the accuracy of the whole process. In the first phase of the experiments, this location was assumed as the mechanical offsets between the optical markers' centers and the center of the US probe piezoelectric sensor strip. These offsets were found using the CAD models which is highly unreliable. This problem was solved during the second design phase.

In the second design of the calibration phantom, two sets of wires are used inside the water tank. First set of wires are the cross-wires for calibration process, located relatively higher inside the tank. For these cross-wire threads, the location of the end points are not symmetric, which means that these threads are woven in the box with wide crossing angles. This gives us ability to get critically diverse readings for our method of calibration. Second set of wires, which contains 7 threads, located at a lower level inside the tank and is used to align the image plane with respect to the tank. These threads are placed parallel to the plane of US image and will be visible as a line in the US image instead of a dot. These threads will be referred to as parallel threads. The mathematical model only uses the cross-wires as only they are used in cross-sectional calibration. Fig. 1 shows the cross-wire threads as well as the parallel threads in the CAD model of the tank.

In order to accurately calibrate the location of the image plane on the probe, a series of images of a thread parallel with the image plane were taken. Each image was 0.1 mm apart; the probe was moved by KUKA Agilus Industrial Robot with high accuracy. The distances in real world coordinates were recorded by Optical Tracking Motion Capture devices. This procedure will be explained in details in Section 2.6.

## *2.3 Selection of Tracking System*

There are four main methods used to track the motion of the components of the system. The first method used is mechanical method in which the probe is attached to a robotic manipulator. The location and orientation of the probe is found by solving the joint angles of the manipulator arm, but the problem is it can only give the information of the probe and not the calibration tank, which is a crucial part for calibration. Acoustic sensors are also used to locate the probe using "Time of Flight" to measure the distance between marker and the transducer. As this system uses sound as a medium so the results get affected by the atmosphere.

The most accurate methods are optical tracking and electromagnetic tracking. Zhang *et al.* [36] and Prager *et al.* [37] have performed the calibration process using electromagnetic tracking and reported RMS error of 0.4 mm to 1.22 mm. Optical tracking system is the most commonly used method for tracking purposes [38, 39, 40]. The calibration process in this thesis used the motion capture system Opti-Track developed by Natural Point. This system outputs the 3 positional coordinates and 3 rotation angles of a rigid body in a 3D space. This 3D space or effective volume is created once in the start when the system is calibrated in one fixed location. A frame is attached to the rigid body when multiple numbers of reflecting spheres are selected as one rigid body. This frame is initially aligned with world frame of the system and gives the angular rotations with respect to this fixed frame. The origin of this frame is placed at the centroid of the rigid body shape.

## *2.4 Calibration of Scaling Matrix*

Matrix transformation representing the Calibration provides the location of the US image pixels in the real-world coordinate system. Optical markers are attached on the calibration tank and on the US probe to collect position and orientation continually.

The tracking system's reference frame is accepted as the world coordinate system.

Fig. 1 depicts the proposed experimental setup. In this figure, $\{W\}$ represents the reference frame of the real time vision based system which is used as the world coordinate system. $\{M\}$ represents the coordinate frame attached to US probe, and $\{T\}$ the frame attached to the calibration tank. A homogeneous transformation with respect to the world coordinates can be written for each frame. In our notation the base frame will be in the superscript. $T_M^W$ represents the marker attached to the US probe with respect to the world coordinate frame, and $T_T^W$ represents the calibration tank marker with respect to the world frame of reference.

The images recorded by the US device, have also a reference frame represented by $\{U\}$. The origin of this frame is the center of the US Probe's sensor array, which coincides with the top center of the US image. The transformation of $\{U\}$ (image) with respect to $\{M\}$ (probe) can be found by measuring the distances. These dimensions can be either obtained from the CAD models of the system, or can be obtained using the parallel threads of the modified calibration tank during the second phase mentioned earlier. The comparison of the results from both phases is given in Section 2.7.

The calibration tank is made out of clear plexi glass and the holes were machined with a CNC milling machine with $3\mu$m accuracy, ensuring accurate dimensions. An optical marker tool is attached to the tank's front wall $\{T\}$ as shown in Figure 1. The position of the threads are referenced to this frame of reference in the model.

A transformation matrix to specify coordinates of the threads that are detected in the US image plane in the world coordinate frame is constructed. Hence, $\mathbf{S}$ is the scaling matrix that contains the scaling factor to convert the pixels to millimeters.

Eq. 1 shows the relation between the points in both planes through the scaling matrix $\mathbf{S}$.

$$p^U = \mathbf{S}T_T^U p^T \tag{1}$$

where $p^U$ are the 2x1 vectors representing the 2D locations of threads in US image plane and $p^T$ represent the locations of threads in calibration tanks frame of reference. $p^U$ has unit in terms of pixels and $p^T$ has the units in millimeters.

Coordinates of the threads in the US image plane are calculated using the US probe's ($T_M^W$) and the tank's ($T_T^W$) positions. $T_T^U$ is found by the following matrix multiplication.

$$T_T^U = T_M^U T_W^M T_T^W \tag{2}$$

where $T_M^U$ is the inverse homogeneous of $T_U^M$ and $T_W^M$ is the inverse homogeneous of $T_M^W$.

The homogeneous transformation $T_T^U$ has 6 unique values to be determined; x, y and z are the position values and can be found in the fourth column of the homogeneous transformation matrix. $\alpha$, $\beta$ and $\gamma$ are the euler angles and can be found by the reverse mapping of the rotation matrix taken out from homogeneous transformation matrix. The scaling matrix has 2 unique values to be determined, $s_x$ and $s_y$ represent the image scaling in the x and y coordinates of the image plane. In total, 8 parameters for the calibration has to be solved.

$$f(\alpha, \beta, \gamma, x, y, z, s_x, s_y) = \mathbf{S}T_M^U T_W^M T_T^W p^T \tag{3}$$

where

$$\mathbf{S} = \begin{bmatrix} s_x & 0 & 0 & 0 \\ 0 & s_y & 0 & 0 \end{bmatrix}. \tag{4}$$

These parameters can be determined by applying the least squares estimation on the collected image data.

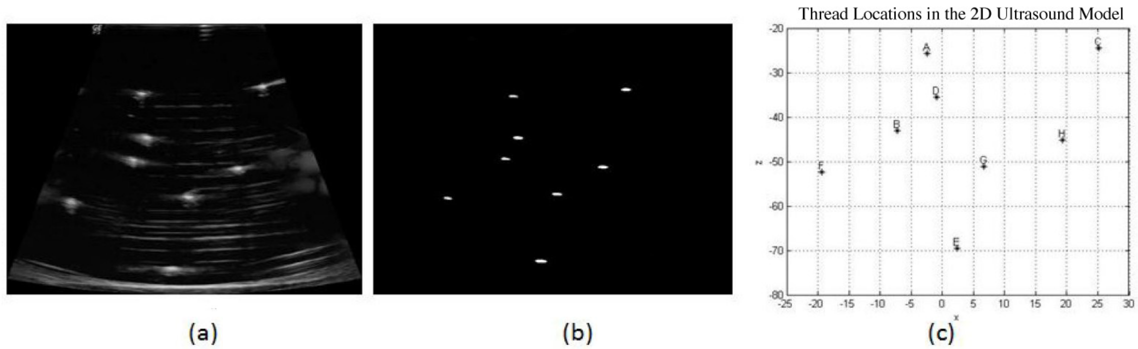


**Figure 3:** (a) US image for the given probe position in the calibration tank. (b) Processed image showing automatically detected thread locations. (c) Thread coordinates from the model for a given position of US Probe.

$$min \sum_{i=1}^{n} ||f_i(\alpha, \beta, \gamma, x, y, z, s_x, s_y) - P_i^U||^2 \tag{5}$$

The final value of the calibration matrix is found by taking the mean over a set of images. Fig. 3 shows an actual ultrasound image and a corresponding thread location plot based on the location of the US probe. Fig 3(a) is the US image recorded at a distance in the tank; Fig 3(b) is the processed image which is segmented in Matlab's normalized cross correlation function [ `normxcorr2.m` ]. Segmented blobs in the image represent the thread locations in the tank, and blob centers give the location of the threads in pixels. Fig 3(c) is the location of the threads with respect to US probe calculated by the mathematical model of the calibration box.

## *2.5 Experimental Setup*

In order to move the US probe in space with 6 DoFs, an industrial manipulator is used. Kuka KR6 R900 (KR Agilus) is the robot that we used and it is capable of moving with 6 DoFs with a minimum step size of 0.1 mm and 0.1° with ±0.03mm repeatability. The US probe is held in a CNC machined holder, which is padded with foam to prevent damage to the probe. This holder will keep the probe in steady position during the experiments.

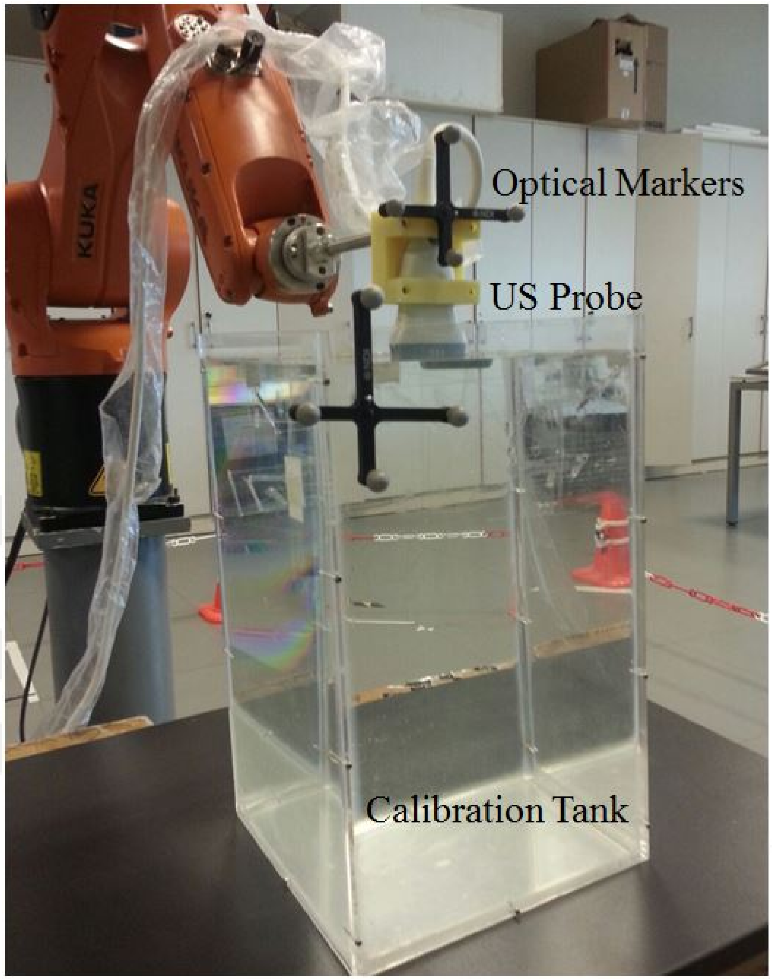


**Figure 4:** US Probe attached to a KUKA KR 6 R900 Sixx while the optical marker data is collected from the water filled calibration tank. A deep calibration tank is used to eliminate the reverberation noise.

GE Logic P5 Ultrasound machine was used to collect data during the experiments. The US machine is connected to the system through Euresys Picolo HD 3G Frame Grabber Card [41]. It streams a video feed at the rate of 15 frames per second. The Optical Tracking system uses 6 infrared cameras to track the optical markers. Natural Point's proprietary software, Motive [42], is responsible for getting feeds from the cameras and send the position and orientation data to Matlab. The software can provide data update rate of up to 120 Hz with an RMS error of less than 1 mm. Fig. 4. shows the experimental setup in which US probe is scanning the phantom tank with the threads. The optical markers of the tank and the probe can also be seen in the Fig. 4.

The Robot manipulator arm is controlled from the computer which is also receiving the US images from the machine. The calibration program, when started, moves the Kuka arm with 0.1 mm step size to sweep the calibration tank. On each step, the US image is stored in the memory with corresponding values of the rigid body coordinates. This data can be later processed using the given equations to find the calibration matrix. For these experiments, 400 images were taken sweeping 4cm for 5 different sets of data each.


**Figure 5:** US Image taken in first design of tank (left) vs US Image taken in second design of tank (right). Reverberations are eliminated.

The first version of the calibration box had 20cm of depth which caused noisy images due to reverberation [43]. The second modified design has a depth of 35cm which eliminated these reverberation artifacts. The images are processed using normalized cross correlation matching algorithm to extract the thread pixels. Fig. 5 shows the US image taken in the second calibration tank and compared to the image taken in the first design of calibration tank. Image on right is quite clear and noiseless. In the first version cotton threads were used while the second version uses fishing wire. The calibration tank is filled with deionized water.

## *2.6 Locating the US Image Plane*

As previously mentioned, the offsets in mechanical fixture of the US probe were calculated from the 3D models. There is a great chance of error as the dimensions of the parts were taken manually. Also the exact location of the image plane on the probes US sensor is not certain. Intuitively it can be understood that this information has great effect on the accuracy of the whole setup because Matlab calculates the thread locations from the mathematical model of the box at precise locations. Fig. 6 shows the modified calibration tank with parallel threads.

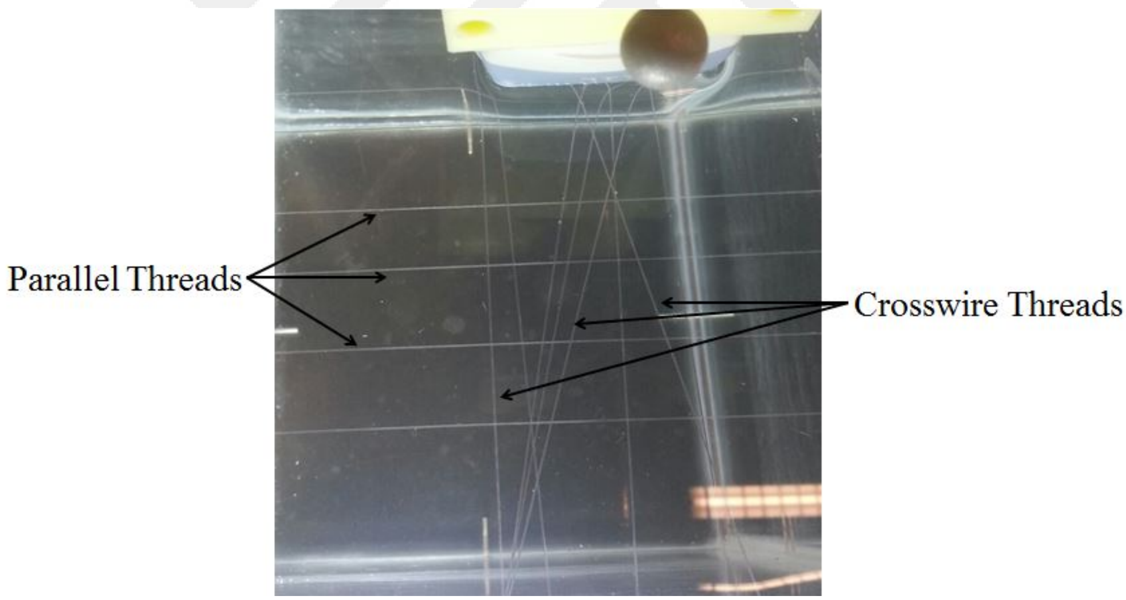


**Figure 6:** Modified calibration tank with parallel threads.

Fig. 7 proposes a way to find the location of US image plane with respect to calibration tanks coordinate frame. In the second design of the calibration tank, parallel threads are introduced. These threads are visible as a line in the image instead of a dot. These thread are at known positions in the tank and are precisely placed with holes drilled with CNC machine. In order to accurately calibrate the location of image plane on the probe, a series of images were taken of a thread parallel with the image plane. Each image was 0.125 mm apart, the probe was moved by KUKA Agilus Industrial Robot with high accuracy. The distances in real world coordinates were recorded by Optical Tracking Motion Capture devices.

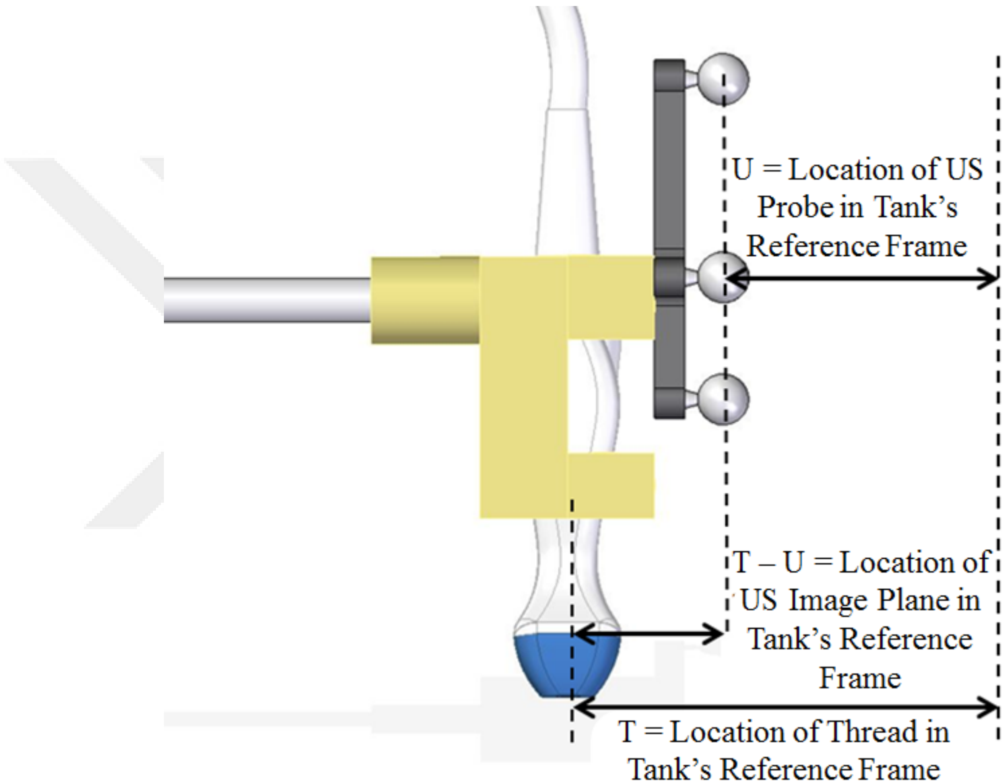


**Figure 7:** Proposed way to find the location of the US image plane.

The distance of the image plane from the optical marker of the probe is found by processing these images. The thread would slowly start to appear in the images and peak the intensity when right on the image plane and again start to fade. The intensity value of this thread is plotted against the distance of US probe from the water tank's optical marker as shown in Fig. 8.

The result was as expected, the intensity of thread starts to increase, reach a peak and declines again until the thread is vanished completely. These readings were taken for different threads in the tank. The distance corresponding to the peak of this plot should represent the distance of the US image plane but the values show some deviation around the mean value over multiple experiments. It can happen due to the vibrations from the robotic arm or changes in apparatus offsets between different experiments. This problem can be solved as shown in Fig. 8, which shows a Gaussian curve was fitted to the data. Fig. 9 shows that the median of the Gaussian gives a better approximation with less deviation from the mean value. The mean results from both maximum peak value and the median of Gaussian converge to same value for larger number of calibration data. The mean of maximum peak was 36.68 mm while mean of medians was 36.71 mm. The value used before was 35.21 mm. The mean result from the Gaussian fit was used for the calibration process because of it small standard deviation over multiple experiments.

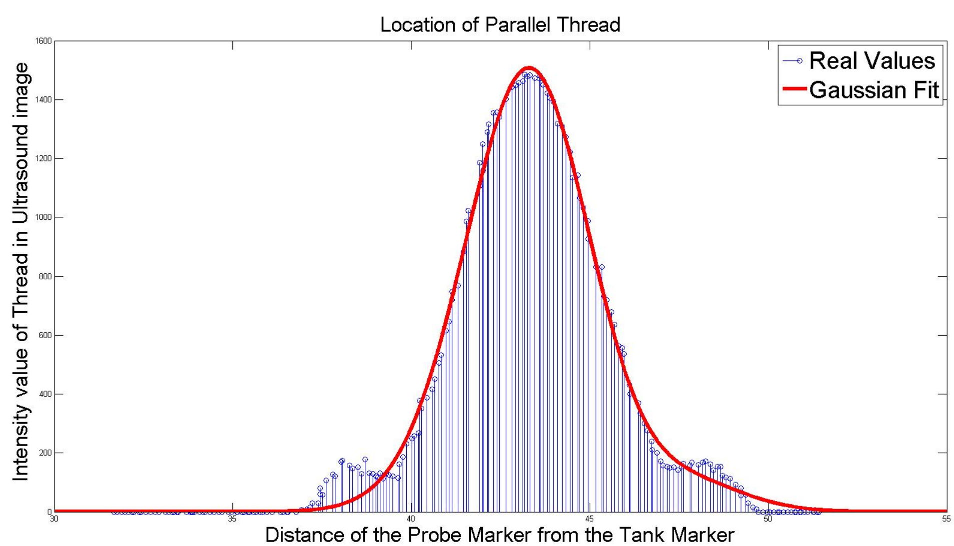


**Figure 8:** Plot of Thread Intensity in US image vs. distance of probe from the tank.

From Fig. 8, the actual location of the thread with respect to optical marker of the tank T is known. Location of the US probe U is also known from the optical tracking system. We can subtract the two distances to find the actual distance of US image plane from the US probe marker as shown in Fig. 7. This calibration process is now robust to offsets caused by physical design of the probe holder mechanism. The calibrations are used directly in the transformation matrices of the whole system to calibrate the space in all three dimensions.

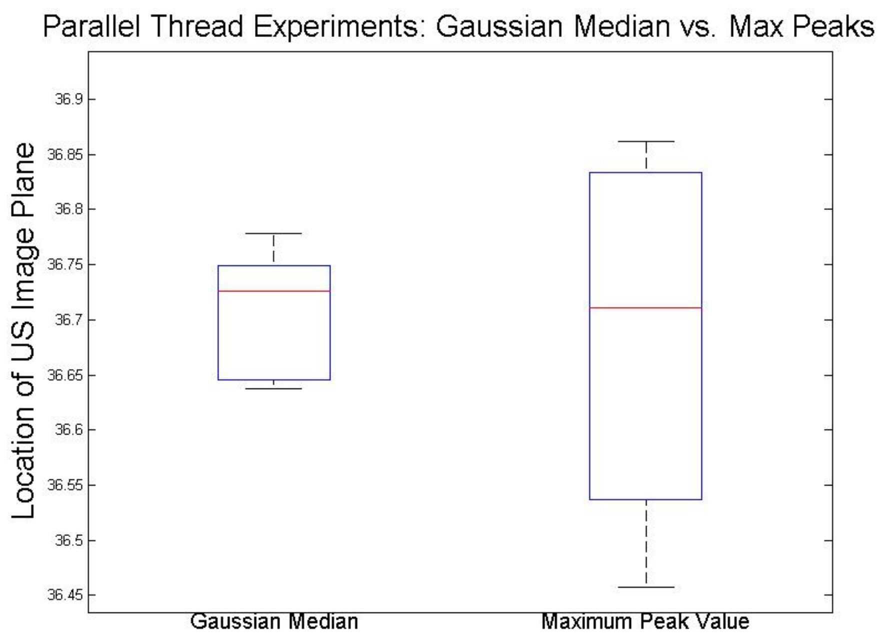


**Figure 9:** Results of Parallel Thread Experiments with their Mean values

## *2.7 Results and Validation*

By using KUKA manipulator's dexterity, image values were taken from various locations at different attitudes. An image processing algorithm detects the threads with known positions as dots in the image, and by cross correlation it compares the positions with the MATLAB model. Table presents the results of the experiments. $s_x$ and $s_y$ are the scaling factors that scale pixels to millimeters. 5 groups with each having 400 images were used to perform the calibration process. Table. 1 shows the results of calibration for three different values of the US plane location. CAD represents the distance found from physical design as discussed in the first design phase, while

Maximum Peak and the Gaussian are found with the help of parallel threads from the second design phase.

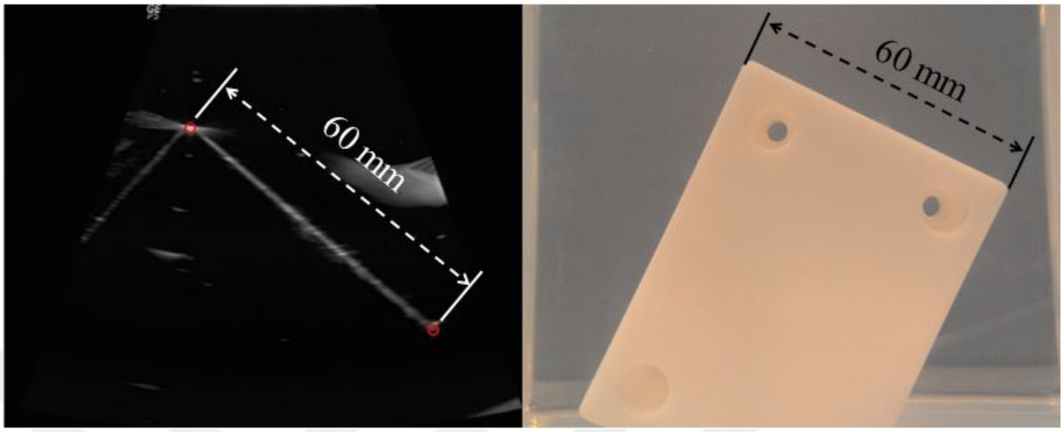


**Figure 10:** Validation Block: US image (left), and the block's image in the water tank (right).

The scaling factors have units of pixels/mm and they convert the robot coordinates from millimeters to pixels. The validation of this calibration is required and can be performed by any of the four main methods described in [36]. This study used the first method, in which the RMS of calibration is calculated. Another way to check for the accuracy of the calibration is to find the dimensions of a known 2D object. Fig. 10 shows a rectangular block and its US image. The length of the side visible in the US image is known to us. The calibration process is validated by finding the distance between the corners as shown in the figure and comparing it with the actual dimension. Table. 1 also shows the RMS error of all three calibration processes. It is clear that the calibration with the parallel threads and Gaussian fit have the minimum RMS error hence the best results.

**Table 1:** Results of calibration with 5 groups of 400 images

| Distance of Parallel Thread | Scaling Factor $s_x$ | Scaling Factor $s_y$ | RMS $s_x$ | RMS $s_y$ | Validation RMS error (mm) |
|---|---|---|---|---|---|
| CAD | 6.40 | 5.71 | 0.94 | 0.83 | 0.17 |
| Max Peak | 6.40 | 5.69 | 0.94 | 0.82 | 0.08 |
| Gaussian | 6.40 | 5.68 | 0.93 | 0.82 | 0.03 |

# CHAPTER III

# SYSTEM ARCHITECTURE

Architecture is the backbone of any complex system. It is the base that defines how a system is divided into subsystems and how they communicate each other to execute tasks. Just like any complex system, architecture is also important in the design of any robotic system such as robotic needle placement system in [44]. The right choice of architecture can lead to meeting system requirements and smooth implementation while a bad choice can cause frustrating problems in the development and can also cause restrictions. [45]

Robotic systems, especially real-time systems, interact with a dynamic environment and have physical components. That's why they require more care when designing as compared to a software system. Mostly systems are designed as a Hierarchical System [46] or a Behavioral System [47] or Hybrid of both [48, 49]. The system architecture adopted for OBR is Hybrid type because it has many subsystems working as independent modules, but controlled by a Master module. All the subsystems or system components are connected as a client-server dependency via UDP networking. The modularity of the system gives it flexibility and more security as each module can be programmed to handle exceptions independently.

In this chapter, each component of the system is discussed as a module and later system integration is presented.

## *3.1 System Components*

OBR is developed to perform needle biopsies on human subjects. Ozyegin Biopsy Robot (OBR) is a 5 degree of freedom robot. In order to make it possible for the OBR to perform autonomous biopsies, other machines and sensors work together with

OBR to make a whole system. Each component has a function of either an actuator or a sensor in the system. Fig. 11 shows the data flow diagram of the robotic biopsy system. It is shown in the figure how the data is flowing between different components of the system.

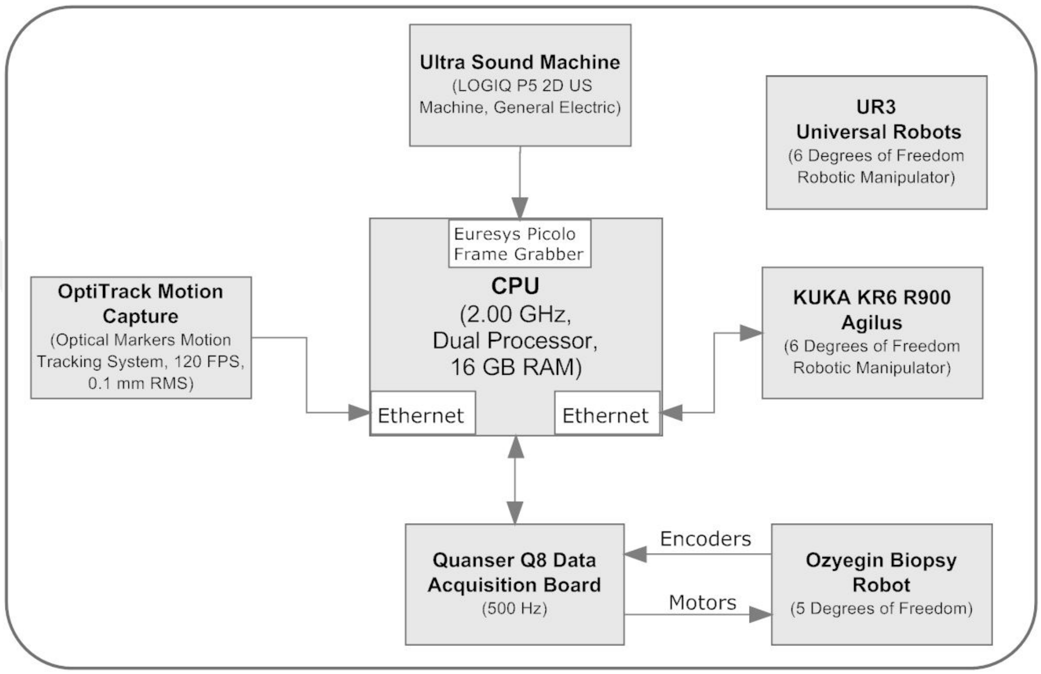


**Figure 11:** Data Flow Diagram

The workstation used in the project as the main CPU has Intel® Xeon® CPU E5-2620 2.00 GHz Dual Processor with 16 GB RAM. The workstation has two Ethernet ports, one of which connects to the Optitrack system and the other one connects to Kuka or UR3 for TCP/IP communications. Optitrack motion capture system is used to track the motion of OBR and the Ultrasound probe in real-time. It uses optical markers and 6 Infrared cameras to track the motion with 6 degrees of freedom. This motion capturing system is also used to calibrate the 2D US images in 3D space which is discussed in detail in chapter II. Kuka and UR3 are robotic arms and are used to manipulate the US probe over in 3D space or move a target phantom alternatively.

The ultrasound machine is used to get the visual feedback for the needle interventions. US machine has the capability to stream the visual data to an external system.

Euresys Picolo Frame Grabber is used to read the video stream, which makes it available in the Matlab. OBR has two way communications with the CPU through the Quanser Q8 DAQ Board. This board reads the encoders from the motors and sends the actuator efforts from the controller to the motors as voltages. Each of the system components are discussed in detail below.

### 3.1.1 OptiTrack Motion Capture

It is shown in the Fig. 11 that how all the parts of the project are communicating with each other and are physically connected. It is also important that all the system components are aware of the physical position of each other to function autonomously and reliably. The motion capture system is used to track the motion of all the moving parts of the project in 3D space. The US probe is attached to Kuka robot's end effector and OBR is expected to perform biopsy on a target point. The US image and the biopsy robot have to be referenced with respect to one common frame of reference in order to get the location of the target point in OBRs frame of reference.

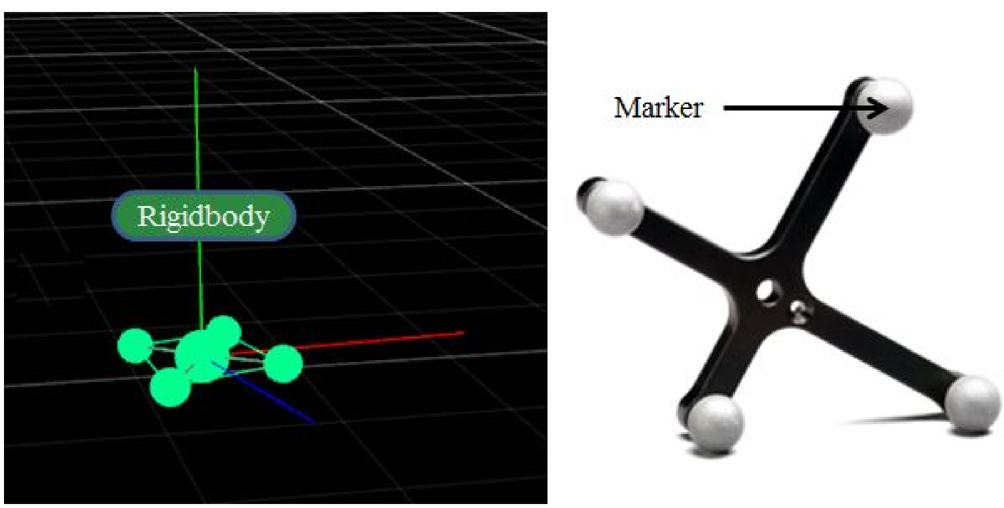


**Figure 12:** Rigidbody with Optical Markers. Image courtesy of NDI Digital

Optical markers are placed on the OBR base frame, US probe and the needle mechanism. These markers form rigid bodies in the Optitrack Software as shown in the Figure. 12. The reflective spheres are called optical markers. The software attaches coordinate frames to each of the rigid bodies and streams the position and orientation of each rigid body to Matlab. Matlab code acquires this information and finds the transformation matrices. These transformation matrices are discussed in detail in chapter II. The new updated software Motive [42], from Natural Point, has reduced RMS error as compared to previous version and has option to solve transformations which saves time on Matlabs side of computations.

### 3.1.2 Ultraosund Machine

In the experiments, a GE LOGIQ P5 2D US machine and a GE 11L linear 2D US probe were used to acquire images. EURESYS PICOLO HD 3G frame grabber is used for data acquisition purposes. US machine sends the video of its screen at the rate of 15 frames per second. These frames contain unnecessary information which is cropped out and only the US image plane is left for processing. An application is programmed to trigger the video stream to acquire the most recent frame when its ready to process new frame.


**Figure 13:** Kuka KR6 R900 sixx. Image courtesy of Kuka Robotics

### 3.1.3 Kuka KR6 R900

KUKA KR 6 R900 sixx is a 6 degree of freedom industrial robotic manipulator. The robot can move in 3D space with minimum step size of 0.1mm translation and 0.1 rotation with less than $\pm 0.03mm$ repeatability. Kuka runs on its controller called KRC (Kuka Robot Controller) which can communicate to an external computer using the TCP/IP protocol. Kuka used in this study can be seen in Figure. 13.

KRC sends an XML file every 12ms to the CPU containing the information about the joint angles and currents and a time stamp. A python application *server.py* receives this data through a UDP socket. The time stamp and relevant data is extracted out of the XML file. *server.py* also sends back a formatted XML file containing the desired values for Kukas joints or end effector to the KRC. The sent message must contain the time stamp of most recent received file. *server.py* also opens a UDP port to listen the desired commands from a third program which can be Matlab or Simulink or any other software capable of UDP communications. Figure. 14 shows the Simulink model that gets six values as input, 3 positions and 3 orientation, and send them in proper format to the *server.py*. The *server.py* application is given in Appendix A.

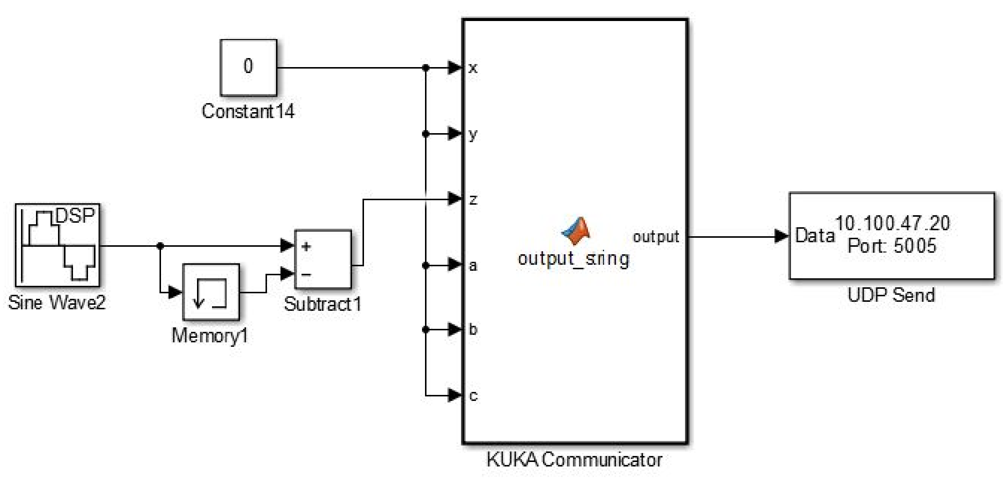


**Figure 14:** Kuka Communication block in Matlab Simulink

### 3.1.4 Universal Robots UR3

Just like Kuka, UR3 is also a 6 degree of freedom industrial arm. UR3 is a small robot as compared to Kuka with a payload of 3 Kg. Its intended use in the project is to manipulate the Ultrasound probe because UR3 can be mounted on the work table due to its small size. UR3 is a collaborative robot and comes with built in force mode control for compliant applications. UR3 runs on its controller called URControl. It can also communicate to an external computer using the TCP/IP protocol similar to Kuka Robot. Universal Robots come with an API which contains all the functional commands of the robot. These commands can be sent to the robot in plain text over an UDP port.

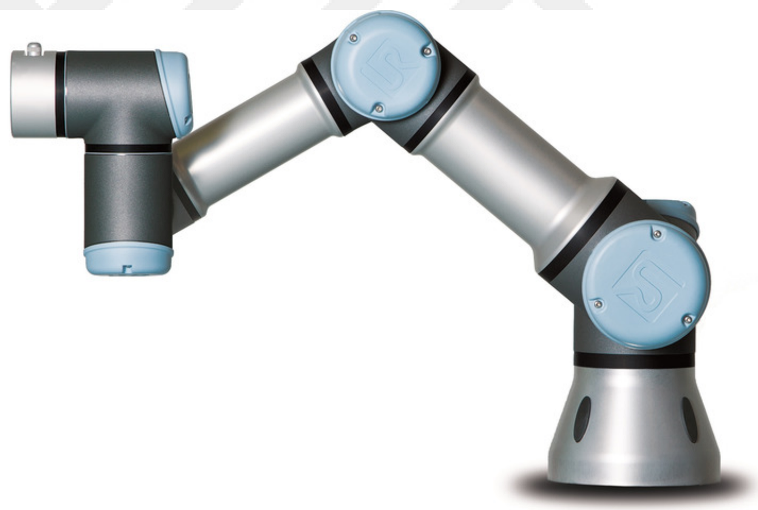

**Figure 15:** Universal Robots UR3. Image courtesy of Universal Robots

### 3.1.5 Ozyegin Biopsy Robot

OBR is a 5 DoF robot designed and developed at Ozu Robotics Lab. The robot has two stages each consisting of a parallel link mechanism with 2 DoF, front stage and back stage as shown in Figure 16. Back stage has an extra rotation at its base giving it 3rd DoF. So there are total 5 DC geared Motors with encoder feedbacks. Quanser Q8 is used as data acquisition board. It reads the values of the encoders and applies voltage to the motors at 500 Hz. The controller for OBR is developed using Simulink according to the control law discussed in [22].

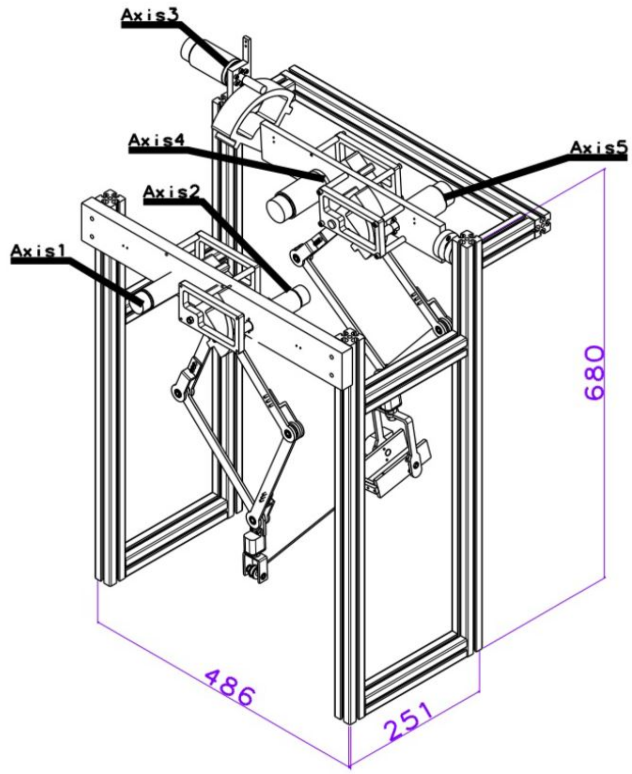


**Figure 16:** Özyeğin Biopsy Robot (OBR)

The OBR controller in Simulink runs parallel to the other parts of the system. It initializes the robot by first calibrating the encoder positions and taking the robot to the home position. At this point the robot is ready to take the needle tip position and insertion angle corrections from an input device or a UDP socket. A snippet from the simulink model is shown in the Figure 17. $OBR\_IK$ is the inverse kinematics of OBR and it takes the correction commands and send correspond joint commands to the OBR motor controllers. The corrections are sent as relative increments or decrements. The function block are processing the commands received from either the UDP port or the Game Controller. The buttons on the Game Controller are used to select between which commands to enable while the Joy Stick on the Game Controller is used to manipulate the needle manually.

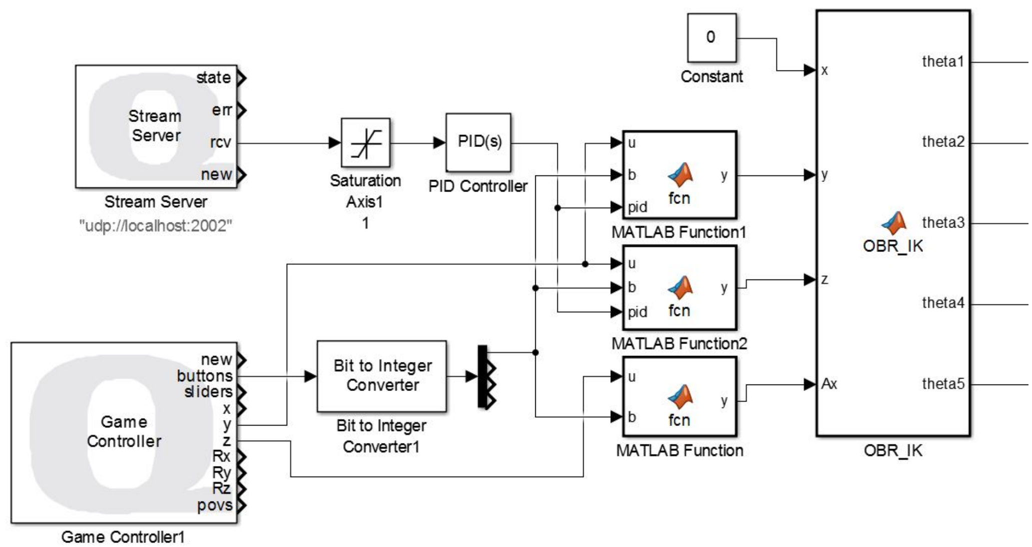


**Figure 17:** Simulink Model for Manual Control or Control through UDP for Özyeğin Biopsy Robot

## 3.2 System Integration

In the previous section the system components are discussed separately and how they are functioning in the system. This section discusses how all the components are integrated together in the system and are running in parallel.

Optitrack motion capture runs on a proprietary software called Motive. The cameras are calibrated in the software using a calibration wand, and then the rigid bodies are created from the optical markers. Once the software starts tracking the rigid bodies, the data streaming is enabled to stream the tracking data in real time to the local or external host. This data can be listened through opening a UDP socket in Matlab.

The python application *server.py* application is started. This piece of code opens two UDP sockets, one to communicate with the KRC through Ethernet port and the other one to receive correction values from another program. As mentioned in earlier sections about *server.py*, it is programmed to receive from KRC every 12ms and then send back the reply with the corrections inside. If the KRC does not receive the reply,

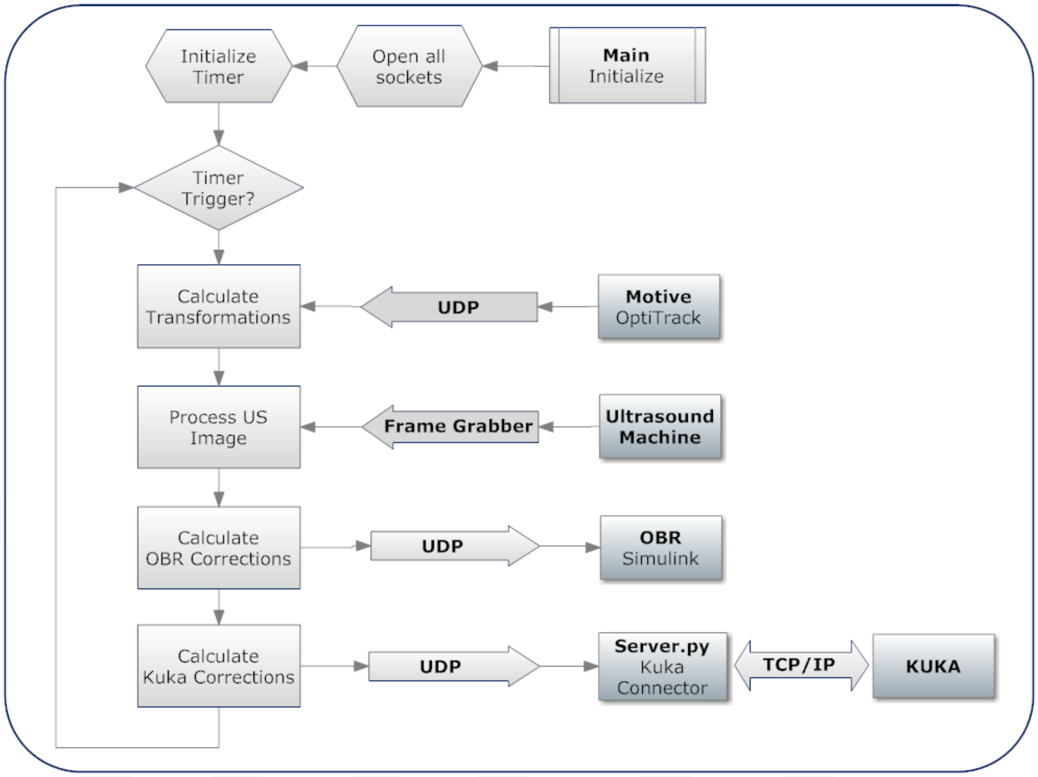


**Figure 18:** Control Flow Diagram

it pings for 100 times and then the communication is lost. Thats why *server.py* is programmed to transmit zeroes as default correction values whenever the external program is not available. It allows it to run in parallel to a program at different frequency of data rates and stay idle while waiting for it to initialize. A similar piece of code is also generated for UR3 with these functionalities.

When the Kuka/UR3 robot and the motion tracking are ready, biopsy robots controller is ran in the Simulink. It has the same mechanism of listening to a UDP socket for correction values from an external program. The controller first finds the joint angles of all the links from the Inverse Kinematics and then Calculated Torque Controller combined with PD Controller computes the motor currents.

Once all the subsystems are open and running, we need one main file, henceforth called as Main Module, which will behave as the Master Program and control the operation of these components and implement the control algorithms for the autonomous needle biopsies. This main module can be programmed in any language or software with UDP support. In this study, Main Module is developed in both Matlab and C++. The control flow diagram of this Main Module is shown in Fig. 18.

After initializing, Main Module connects to the UDP sockets that are opened for communicating with Motive, OBR and *server.py*. In order to run the main at a constant rate, a timer interrupt is initialized which will trigger the main loop at constant intervals of time. The frequency of this timer is set manually and depends on the processing time taken to complete one cycle. Once the timer is triggered, first of all the tracking data is received and transformations are calculated. After that the US video object is triggered to get the latest frame and this frame is processed to find the location of the target point using the calibration factors found in chapter II. At this point the information from both these sensory inputs is used to generate the corresponding correction values for both OBR and Kuka/UR3 and transmitted through the respective sockets. And then the program waits here for the next trigger of the timer.

On average one loop of instructions between timer-callbacks take 0.1 seconds making 10 loops per second as the maximum frequency of execution. In order to achieve more efficiency, image processing algorithms are implemented in a separate C++ code with OpenCV Library. By doing this, computational time was decreased on the Matlab's side allowing the program to run at 15 Hz hence utilizing the full capacity of US machine.

# CHAPTER IV

# MOTION COMPENSATION

One of the targets of this study was to make an autonomous robotic biopsy system. In order to be autonomous, the system must be able to interact with its environment and behave accordingly. The level of autonomy can vary for different systems and may depend on many factor like task complexity, environment dynamics and human supervisor dependency [50]. Any autonomous system must be able to detect any change in the parameters it controls through a feedback and react to the change. In our case, the needle must reach a target tissue which is a dynamic environment due to constantly changing position. US imaging provides the visual feedback. This chapter discusses about the motion compensation between the moving target and the needle tip position.

OBR is designed to perform biopsies in the abdominal regions. The organs inside the patient's body move due to respiratory or voluntarily movements of the patient. A tumorous tissue can also move from its place due to US probe pressure on skin and needle insertion. Vishnu *et al.* [51] solved the problem by stabilizing the breast with external actuators in order to align tumor with needle path. Their study shows how needle insertion interact with the tissues changes the location of the target. external pressure is applied to re-align the target with the needle path. But this technique can cause damage to healthy tissues.

This study suggests a method in which the robot moves the needle with the moving target in order to cancel the relative motion. Sharma *et al.* [52] and Schwiekard *et al.* [53] have concluded in their studies that motion compensation of a respiratory motion is achievable. Riviere *et al.* [54] presented an adaptive controller which was able to model and predict the breathing motion of a target during needle interventions. Trejos *et al.* [55] discussed about the ability of a platform which allowed the surgeon to perform tasks on a motion-cancelled target.

In this chapter, two different control techniques to track a moving target are presented. One is a simple PD controller and the other is Receding Horizon Model Predictive Control [56] (or simply called Model Predictive Control (MPC)) . The second technique utilizes the known model of the breathing motion which will be discussed in the Section 4.2.

## 4.1 Moving Target

In order to develop a controller for motion compensation, a moving target is needed. In our study a water tank was used as a phantom with a robotic arm moving a target object. A 20x20 *mm* piece of rubber was used as the target because its appearance in US image was good for segmentation algorithm. This piece of rubber is attached at the end of Kuka robotic arm with an extension rod and it can be moved with any given reference signal. Figure. 19 shows the real target and the US image of the target and the needle being tracked by the image processing software.

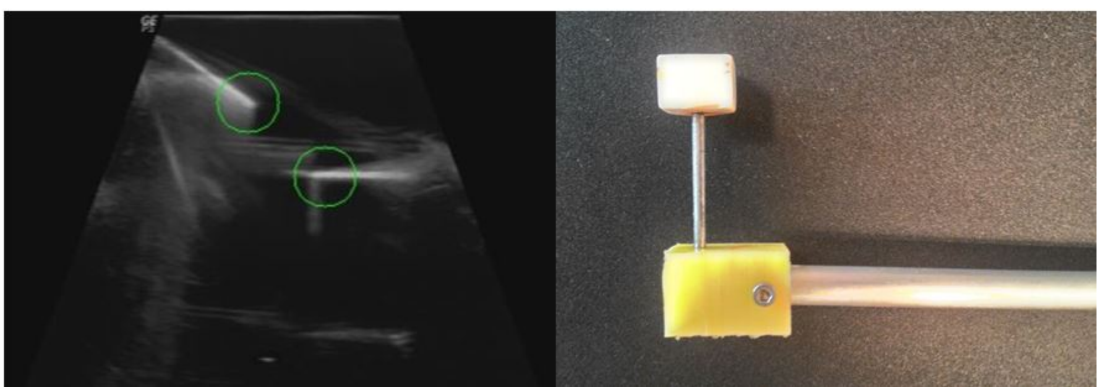

**Figure 19:** Rubber Target and needle in US image. Rubber Target attached to the extension rod at the end effector of Kuka

Reference signal for the target motion to Kuka is sent from the external system and runs outside of the main OBR system loop. That's why OBR system does not have any information about the motion except from the visual feedback. The following sections shows how the breathing motion is estimated to generate a reference signal for tracking purposes.

## *4.2 Breathing Motion Model*

Breathing patterns can change person to person, and even in different conditions of a same person. The body deformity due to breathing depends on body type and breathing type. Different parts of abdomen and chest deform as we breathe. The deformity is not only external, internal organs move with different patterns due to breathing. This breathing pattern can be modelled and this information can be used to improve the tracking performance.

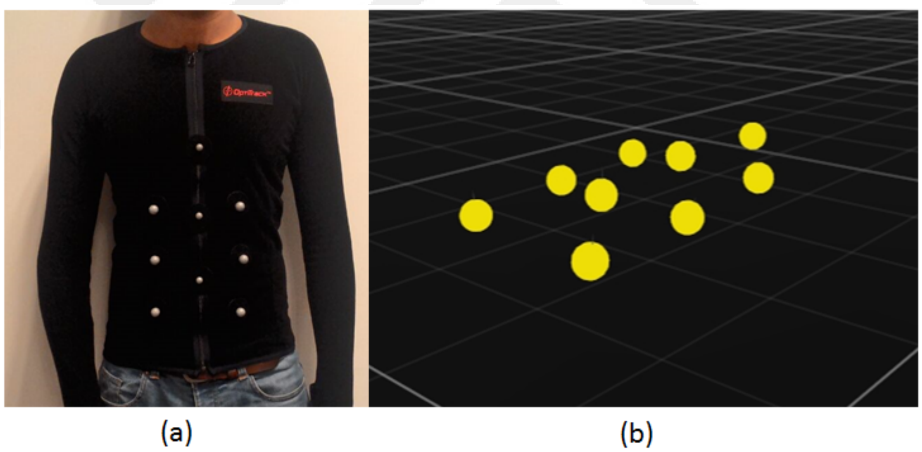

**Figure 20:** Optical markers placed on human body: (a) Optical Marker Placement. (b) Optical Markers in Motive Software

There are many ways suggested in literature to record breathing data of a human subject. This study used the motion tracking system to record the motion of 9 different points on the chest and abdomen of human subjects. Optical markers were placed on 9 different points on the subjects front as shown in Figure 20. The subjects were asked to lie down on a flat table and breathe calmly. The point with most complicated motion and higher amplitude was chosen to model the breathing motion.

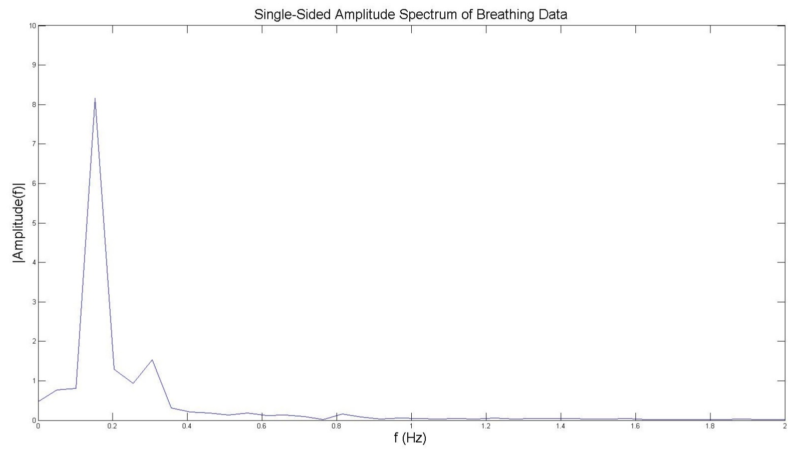


**Figure 21:** Amplitude Spectrum of Breathing Data

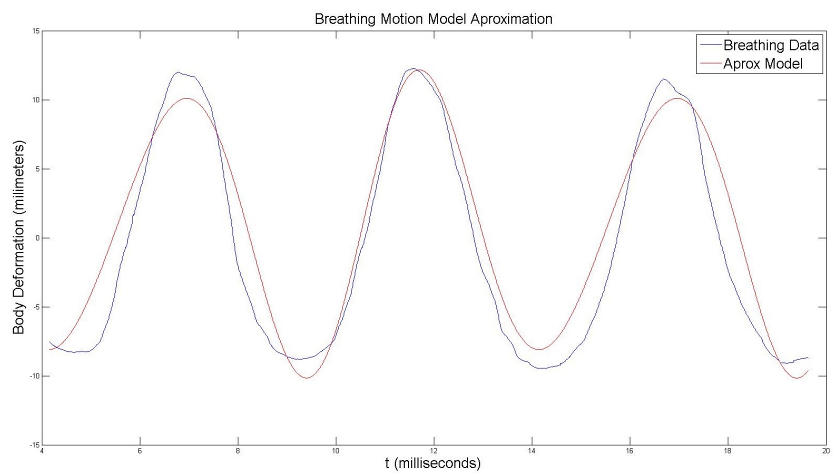


**Figure 22:** Breathing Motion Model vs Actual Data

The breathing motion is modelled by taking the Fourier Transform of the recorded data. Figure 21 shows the amplitude spectrum of the recorded breathing motion data. It can be seen that the spectrum has two peaks at 0.2 Hz and 0.3 Hz. The breathing motion can be approximated using these two frequencies as shown in Eq. 6. Breathing modelled data and the actual breathing can be seen in Figure. 22.

$$8\ \sin(2\pi(0.2)t) + 1.5\ \sin(2\pi(0.3)t) \tag{6}$$

### *4.3 PD Controller*

The purpose of tracking a target tissue is to cancel the relative motion between target and the needle tip to perform accurate biopsies. It would be naive to assume a target tissue to be stationary while performing biopsies on a patient. So a controller is needed to control the motion of the needle tip and track the path followed by the target tissue. One of the simplest controllers that can be used in this situation is a PID controller. The feedback of both the needle tip and the target from the US imaging is available, also shown in Figure 19. The image processing algorithm developed in [24] is used to get the position of both needle tip and moving target in real time. This algorithm is developed in C++ using OpenCV for maximum frames per second capacity. The error between the position of target and the needle tip is sent to the OBR controller via UDP connection in real time which than uses it to generate command signals for the OBR to reach the targets position using PD controller. The Integral parameter was not used so it is simply a PD controller. The control flow of the system is showed in Figure. 23.

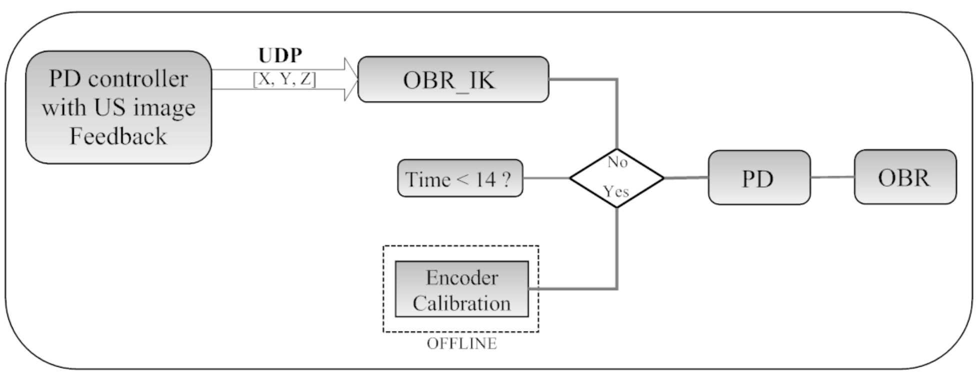


**Figure 23:** Motion Compensation with PD Control

For the first 14 seconds, all the links of the OBR go to an initial position whose angle is known. The values of the encoders are noted and the encoder offsets are corrected. This is called encoder calibration process [22]. The motor commands for the duration of calibration are calculated offline and stored in *Encoder Calibration* data matrices. A clock switch switches the command control between the PD controller and the encoder calibration values at 14 seconds of running time.

The algorithm is tested at frequencies of 0.2 Hz to 1 Hz and peak to peak amplitudes of 1 cm to 3 cm. Figure 24 shows the tracking of a target motion with 0.2 Hz and 1 cm amplitude. The motion was at an angle hence it was 2 dimensional. It shows plots for both X and Y direction.

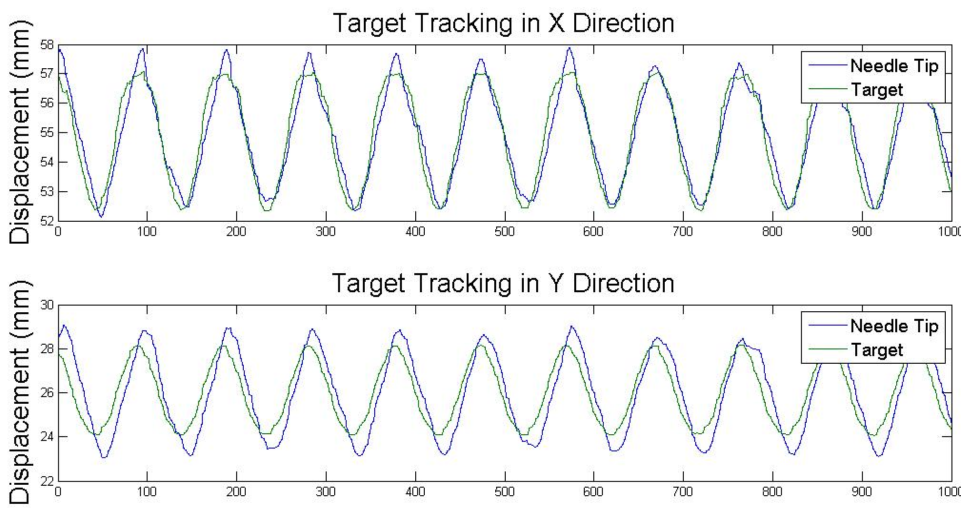


**Figure 24:** Motion Tracking with PD Control

The RMS errors are 0.81 mm and 0.42 mm for Y and X direction respectively. The reason for this high RMS error is processing time of images between the updates to the controller effort. This is also one of the reasons this controller is not suitable for higher frequencies. Sensor delay, which is discussed in the following section is also contributing to introduce lag in tracking.

## *4.4 Sensor Time Delay - US Imaging Latency*

All the sensors have some intrinsic latency in them which is the time delay between the actual event and the time when sensor reports the event. In motion compensation application of OBR, US Imaging is our feedback system. The Ultrasound machine takes some time to process the information received from the piezoelectric sensors in the sensor array. Once a frame of US image is created in US machine, it is than transmitted to the main computer using VGA cable and Frame Grabber card.

All these processes take some time to execute in reality. Ignoring this time delay can cause large tracking errors as the target will move to a new position by the time current US image will be registered by the main computer. An experiment is designed to measure the sensor delay and incorporate it in our control scheme.

The needle tip of OBR is controlled with a joystick and moved randomly. US imaging is used to record the motion of the needle. Both of the events are time stamped using a same universal clock. The commands to OBR are stored with a time stamp right before sent to the robot after all the processing. The time stamp for US image is used right when a new frame is triggered before performing any processing. In this way, the computational delays of Matlab are eliminated and the offset between two sets of data should purely be because of US machines processing time. Fig. 25 shows the plots of both data sets. The delay between the two signals is clearly visible and calculated to be 150 ms.

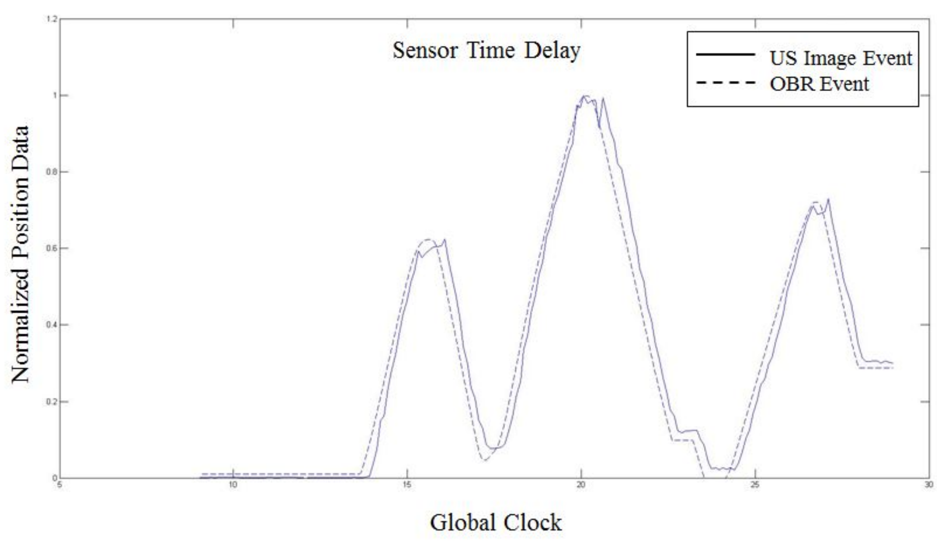


**Figure 25:** US Imaging Latency

## 4.5 Receding Horizon Model Predictive Control

The results of tracking from feedback control were promising and below the acceptable error of 1 mm RMS. But this controller is expected to cross this safe limit of error on higher frequency of target motion. OBR is designed to have the capability of tracking a target moving with 2 Hz frequency and 10 mm amplitude. Also the sensor latency found in the previous section introduces a phase lag in the tracking. Design of a new controller is needed which can handle these problems. This section presents the design of a Model Predictive Control (MPC) [56] which utilizes the information of breathing model and sensor delays to optimize tracking problem.

Model Predictive Control optimizes the current state of the system taking the future states in account. A number of samples, for instance $N$, are selected as a design parameter, also called as Horizon, and the current state of the system is optimized over this Time-Horizon. The current state is optimized over $[k, k + N]$ samples, $k$ being the current sample, but only the current position is implemented. For the next position in time, the horizon is moved forward and the state is optimized over $[k+1, k+N+1]$. This gives this technique the name of Receding Horizon Model Predictive Control (RHMPC) [57]. The length of the horizon is finite for periodic systems. The breathing model is a periodic signal hence one cycle can be used as Feedforward signal for the next cycle.

RHMPC is an iterative and multivariable process which uses the dynamic model of the system, history of previous control efforts and an optimization cost function over the length of horizon. The dynamic model of each joint of OBR is available as calculated during the system identification presented by Orhan *et al.* in [22].

$$x[k+1] = \mathbf{\Phi} x[k] + \mathbf{\Gamma} u[k] \tag{7}$$

$$y[k] = \mathbf{H} x[k] \tag{8}$$

Using the breathing model of previous cycle for prediction, a cost function can be defined and an Optimal Control can be designed to minimize the cost function.

$$J[k] = \sum_{k=k_0}^{k_0+T} \Big( (x[k] - x_{est}[k])^T \mathbf{Q} \big(x[k] - x_{est}[k]\big) + u^T[k]\mathbf{R}u(k) \Big) \tag{9}$$

$$x_{est} = \mathbf{L} y_{est} \tag{10}$$

$$L = H^T(HH^T)^{-1} \tag{11}$$

$$Q = (I - LH)^T Q_1 (I - LH) + H^T Q_2 H \tag{12}$$

The optimal tracking problem goal is to find optimal control $u$ for the system that will minimize the given cost function in Eq. 9. This will result in y tracking the signal $y_{est}$. $\mathbf{Q}$, $\mathbf{Q_1}$ and $\mathbf{Q_2}$ are non-negative definite symmetric matrices and $\mathbf{R}$ is a positive definite symmetric matrix. When solved as Optimal Feedback Regulator [58, 59], the solution to this control problem becomes as follows:

$$u[k] = -\Big(\mathbf{\Gamma}^T \mathbf{S}[k+1]\mathbf{\Gamma} + \mathbf{R}\Big)^{-1} \mathbf{\Gamma}^T \Big(\mathbf{S}[k+1]\mathbf{\Phi}x[k] + \mathbf{M}[k+1]\Big) \tag{13}$$

Here, $\mathbf{S}$ and $\mathbf{M}$ are iterative equations:

$$\mathbf{S}[k] = \mathbf{\Phi}^T \Big(\mathbf{S}[k+1] - \mathbf{S}[k+1]\mathbf{\Gamma}(\mathbf{\Gamma}^T\mathbf{S}[k+1]\mathbf{\Gamma} + \mathbf{R})^{-1}\mathbf{\Gamma}^T\mathbf{S}[k+1]\Big)\mathbf{\Phi} + \mathbf{Q} \tag{14}$$

$$\mathbf{M}[k] = \Big(\mathbf{\Phi}^T + \mathbf{K}^T[k]\mathbf{\Gamma}^T\Big)\mathbf{M}[k+1] - \mathbf{QL}y_{est}[k] \tag{15}$$

and $\mathbf{K}$:

$$\mathbf{K}[k] = -\Big(\mathbf{\Gamma}^T\mathbf{S}[k+1]\mathbf{\Gamma} + \mathbf{R}\Big)^{-1} \mathbf{\Gamma}^T\mathbf{S}[k+1]\mathbf{\Phi}\ . \tag{16}$$

The resulting control algorithm is composed of feedback and feedforward parts which are identified, respectively, as follows:

$$u_{fb}[k] = -\left(\mathbf{\Gamma}^T\mathbf{S}[k+1]\mathbf{\Gamma} + \mathbf{R}\right)^{-1}\mathbf{\Gamma}^T\,\mathbf{S}[k+1]\mathbf{\Phi}x[k] \tag{17}$$

$$u_{ff}[k] = -\left(\mathbf{\Gamma}^T\mathbf{S}[k+1]\mathbf{\Gamma} + \mathbf{R}\right)^{-1}\mathbf{\Gamma}^T\,\mathbf{M}[k+1] \tag{18}$$

such that:

$$u[k] = u_{fb}[k] + u_{ff}[k]\ . \tag{19}$$

*Implementation:* The breathing motion model found in Section 4.2 is used as the reference signal for the RHMPC. The same target object used in the PD tracking is used for RHMPC tracking. Kuka is programmed to follow the trajectory of modelled data. Same signal is fed to the RHMPC as well to control the needle tip motion. In order to synchronize both signals, phase difference must be calculated.

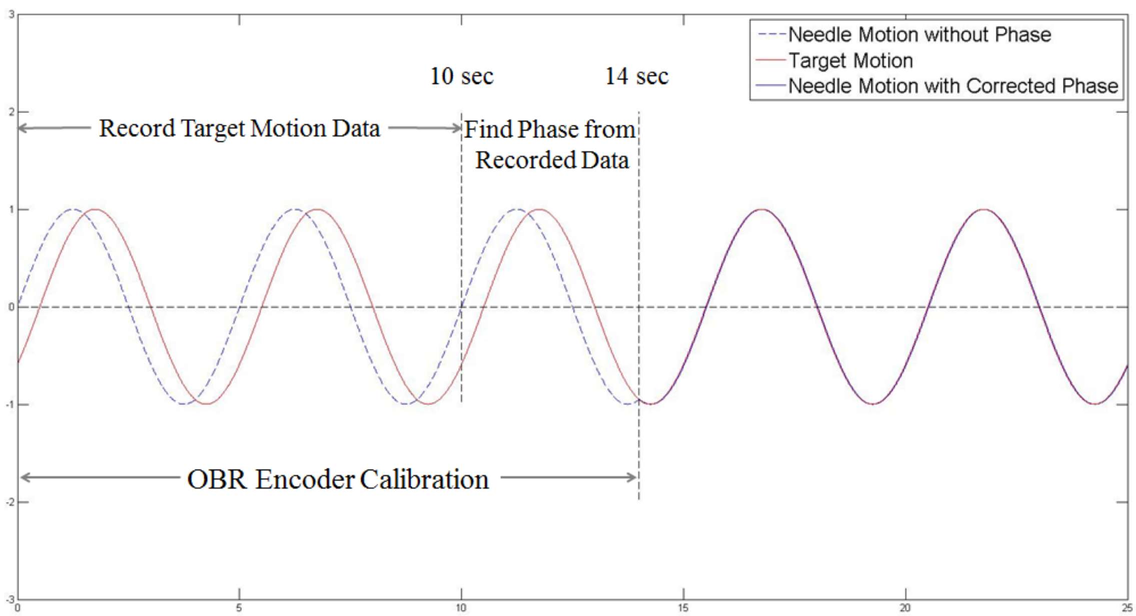


**Figure 26:** Timeline of Phase Offset detection

As mentioned earlier, OBR follows a predefined trajectory for the first 14 seconds. In this time the encoders are being calibrated and no control algorithm is enabled. This time can be utilized to find the phase offset of the target motion and added to the input signal of RHMPC. Another thread of Matlab is started in parallel to the

OBR controller. This thread waits for an enabling signal from the OBR controller in order to synchronize the clock. Figure 26 shows how the phase is calculated and added to the input signal.

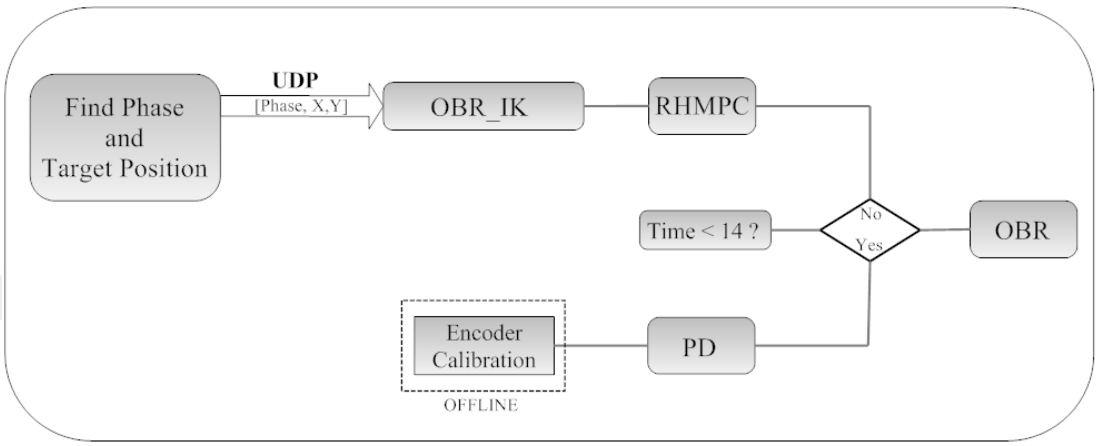


**Figure 27:** Control Flow of RHMPC

At time zero, the data of target motion starts to get stored. The data is stored for 10 seconds which is enough to get two complete waves of the lowest frequency tried with maximum amplitude which is 0.2 Hz. At this point, a sinusoidal function can be fitted to the recorded data using least square fit. From this fit, the phase of the target motion can be found. The mean position of target motion to align the needle tip with it can also be found. This information is than shared with the OBR controller using a UDP connection before the 14 second mark hits. Hence at 14 seconds, the input signal phase to the RHMPC is corrected and it starts to track the target perfectly. Figure 27 shows the control flow of RHMPC with phase correction.

The Kuka robot is programmed to move the target in a sinusoidal pattern. The algorithm is tested at frequencies of 0.2 Hz to 1 Hz and peak to peak amplitudes of 1 cm to 3 cm. Figure 28 shows the tracking of a target motion with 1 Hz and 1 cm amplitude with an RMS error of 0.2673 mm.

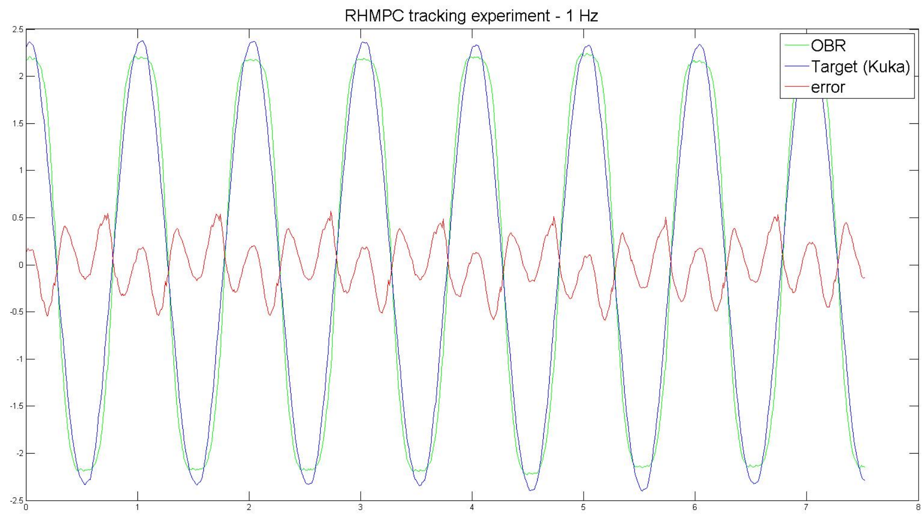


**Figure 28:** RHMPC Target Tracking

## *4.6 Comparison of RHMPC with PD*

It can be seen that the RMS error of PD controller for motion compensation is quite higher as compared to RHMPC but within the acceptable value of 1 mm. RHMPC was able to overcome the problems faced by a typical PID controller and provided more stability and reliability with RMS less than 1 mm. Figure 29 shows the comparison of the errors of these tracking control solutions. It can clearly be seen that the errors in case of RHMPC are contained well under the safe value of 1 mm with mean very close to zero which indicates perfect phase synchronization. On the other hand PD controller has a constant lag while tracking which causes the mean of error to move away from the zero value.

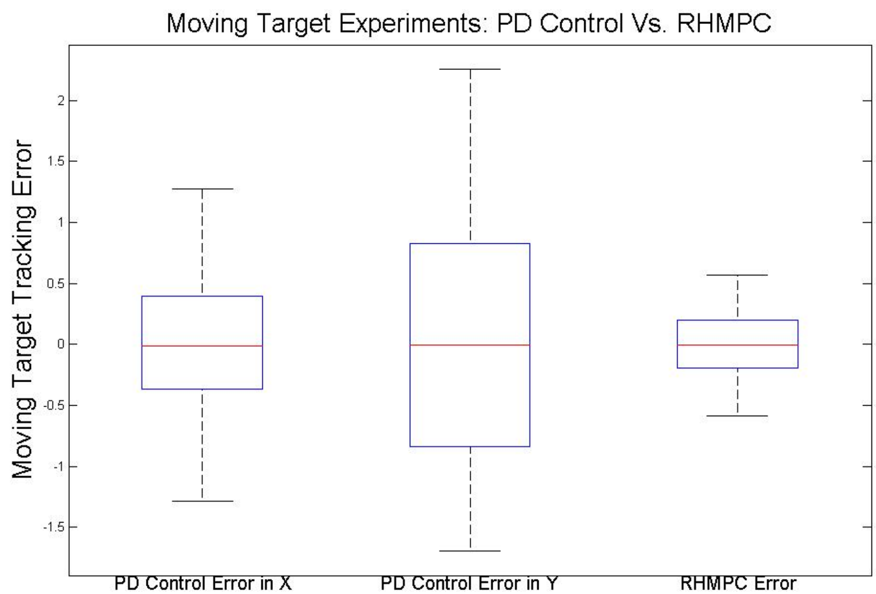


**Figure 29:** Tracking results of RHMPC and PD Controller

# CHAPTER V

# CONCLUSION

This thesis presented design and implementation of the architecture of a robotic system for autonomous biopsy procedures. The robotic system is designed to perform biopsies on a phantom with a moving target. It is capable of tracking the motion of a target by keeping the relative motion between it and needle tip as close to zero. This task is also referred as motion compensation. The system was tested to perform biopsy on a target which was moving at 1 Hz frequency and 10 mm amplitude.

In order to design the controller of OBR to perform tracking tasks, a visual feedback is needed. Ultrasound imaging provides a safe, cheap and reliable visual feedback solution. A calibration process of US images is needed to convert pixels to millimeters. A novel technique of calibration was proposed, using a calibration tank with crosswire threads and also parallel threads. The proposed calibration process has RMS error of 0.03 mm.

US images with the validation block were taken at different angles in order to validate the calibration process. These validation results were found to be within 0.1 mm of actual dimensions of the validation block on average. The accuracy of the calibration process largely depends on the motion tracking system, which has an RMS error of 0.1 mm to 1 mm depending on the careful placement of cameras. The current calibration scheme serves the purpose for this project and is only limited by the capabilities of external sensors like US machine and motion tracking system.

Özyeğin Biopsy Robot's system architecture is designed in a way that all the system components exist as modules and one Master program controls the execution of tasks. The Master program is connected with the subsystem modules over a client-server dependency via UDP networking. The subsystems have have ability to run independently in case of Master failure which makes the system secure and flexible.

In order to track a moving target, both Feedback and Feedforward controllers were designed. Feedback control with PD gains performed just around the minimum design requirement which is 1 mm RMS tracking error. PD controller showed RMS error of 0.95 mm. Feedback Controller is not expected to perform well under higher frequencies of target motion and also due to sensor latency.

To handle the higher frequencies and dynamic behavior of the operation environment, a Model Predictive Control is implemented. Sensor time latency was found through experiments and breathing motion was modelled to design the Receding Horizon MPC. The performance of the RHMPC was found to be very promising with a tracking RMS error of 0.23 mm at 1 Hz.

# APPENDIX A

# SERVER.PY

```python
import socket
#import settings
import time
import select
import string
import re
import struct
import sys
from array import *
import xml.etree.ElementTree as ET

from generateTrajectory import Trajectory

SERVER_IP = '10.100.48.101'
LOCAL_IP = '10.100.47.20'
BUFFER_SIZE = 1024
SERVER_PORT = 49152
MATLAB_PORT = 5005
HEADER = '<Sen Type=\"ImFree\"><EStr>KRCnexxt - RSI Object ST_ETHERNET</EStr>'
FOOTER = '<Tech T21=\"1.09\" T22=\"2.08\" T23=\"3.07\" T24=\"4.06\" T25=\"5.05\" T26=\"6.04\" T27=\"7.03\" ' \
        'T28=\"8.02\" T29=\"9.01\" T210=\"10.00\"/><DiO>125</DiO><IPOC>0000000000</IPOC></Sen>'

def parseData(data):
    parser = ET.XMLParser(encoding="utf-8")
```

```
    tree = ET.fromstring(data, parser=parser)
    angles = tree.find('RIst').attrib        # this is angles in axis mode, xyzabc in cart. mode
    refAngles = tree.find('RSol').attrib    # same here
    currents = tree.find('MACur').attrib    # currents
    tiem = time.clock()
    if False :
        parsedData = '{} {} {} {} {} {}'.format(currents['A1'], currents['A2'], currents['A3'], currents['A4'], currents['A5'], currents['A6'])
    if True :
        parsedData = '{} {} {} {} {} {} {}'.format(angles['X'], angles['Y'], angles['Z'], angles['A'], angles['B'], angles['C'], tiem)
    if False :
        parsedData = '{} {} {} {} {} {}'.format(angles['A1'], angles['A2'], angles['A3'], angles['A4'], angles['A5'], angles['A6'])
    return parsedData

def create_command_string(command_list):
  correctionString = '<RKorr X=\"{}\" Y=\"{}\" Z=\"{}\" A=\"{}\" B=\"{}\" C=\"{}\" />'.format(*command_list)
  # correctionString = '<AKorr A1=\"{}\" A2=\"{}\" A3=\"{}\" A4=\"{}\" A5=\"{}\" A6=\"{}\" />'.format(*command_list)
  # print correctionString
  return HEADER + correctionString + FOOTER

def main():
  sockKuka = socket.socket(socket.AF_INET, socket.SOCK_DGRAM)  # Create a UDP socket
  sockKuka.bind((SERVER_IP, SERVER_PORT))

  sockMatlab = socket.socket(socket.AF_INET, socket.SOCK_DGRAM)
```

```
  sockMatlab.bind((LOCAL_IP, MATLAB_PORT))

  my_data = array('d',[0,0,0,0,0,0])
  while True:
    inready, outready, exready = select.select([sockKuka, sockMatlab], [], [])
    #my_data = [0,0,0,0,0,0]
    for s in inready:

      if s == sockMatlab:
        data, socket_of_matlab = sockMatlab.recvfrom(BUFFER_SIZE)
        data = struct.unpack('!6d',data[0:48])

      if s == sockKuka:
        received_data, socket_of_krc = sockKuka.recvfrom(BUFFER_SIZE) # buffer size is 1024 bytes
        parsedData = parseData(received_data)
        #print parsedData
        data_to_send = create_command_string(data)
        #print data_to_send
        data_to_send = re.sub('<IPOC>.*</IPOC>', re.search('<IPOC>.*</IPOC>', received_data).group(0), data_to_send) #set timestamp
        sockKuka.sendto(data_to_send, socket_of_krc)

if __name__ == '__main__':
    main()
```

# Bibliography


[1] C. Kim, D. Chang, D. Petrisor, G. Chirikjian, M. Han, and D. Stoianovici, "Ultrasound probe and needle-guide calibration for robotic ultrasound scanning and needle targeting," *IEEE Transactions on Biomedical Engineering*, vol. 60, no. 6, pp. 1728–1734, 2013.

[2] K. M. Pondman, J. J. Fütterer, B. ten Haken, L. J. S. Kool, J. A. Witjes, T. Hambrock, K. J. Macura, and J. O. Barentsz, "Mr-guided biopsy of the prostate: an overview of techniques and a systematic review," *European urology*, vol. 54, no. 3, pp. 517–527, 2008.

[3] H. Zaidi, Y. Chao, Z. Lei, and Y. Wang, "Design and optimization analysis of open-mri compatibile robot for neurosurgery," in *Bioinformatics and Biomedical Engineering, 2008. ICBBE 2008. The 2nd International Conference on*, pp. 1773–1776, IEEE, 2008.

[4] N. Tanaiutchawoot, C. Wiratkapan, B. Treepong, and J. Suthakorn, "On the design of a biopsy needle-holding robot for a novel breast biopsy robotic navigation system," in *Cyber Technology in Automation, Control, and Intelligent Systems (CYBER), 2014 IEEE 4th Annual International Conference on*, pp. 480–484, IEEE, 2014.

[5] B. Yang, U. Tan, A. McMillan, R. Gullapalli, J. P. Desai, *et al.*, "Design and implementation of a pneumatically-actuated robot for breast biopsy under continuous mri," in *Robotics and Automation (ICRA), 2011 IEEE International Conference on*, pp. 674–679, IEEE, 2011.

[6] A. Majewicz, S. P. Marra, M. G. van Vledder, M. Lin, M. A. Choti, D. Y. Song, and A. M. Okamura, "Behavior of tip-steerable needles in ex vivo and in vivo tissue," *Biomedical Engineering, IEEE Transactions on*, vol. 59, no. 10, pp. 2705–2715, 2012.

[7] Y. Moon and J. Choi, "A compliant parallel mechanism for needle intervention," in *Engineering in Medicine and Biology Society (EMBC), 2013 35th Annual International Conference of the IEEE*, pp. 4875–4878, IEEE, 2013.

[8] G. S. Fischer, I. Iordachita, C. Csoma, J. Tokuda, S. P. DiMaio, C. M. Tempany, N. Hata, and G. Fichtinger, "Mri-compatible pneumatic robot for transperineal prostate needle placement," *IEEE/ASME transactions on mechatronics*, vol. 13, no. 3, pp. 295–305, 2008.

[9] R. Seifabadi, N. B. Cho, S.-E. Song, J. Tokuda, N. Hata, C. M. Tempany, G. Fichtinger, and I. Iordachita, "Accuracy study of a robotic system for mri-guided prostate needle placement," *The International Journal of Medical Robotics and Computer Assisted Surgery*, vol. 9, no. 3, pp. 305–316, 2013.

[10] J. Chung, H.-J. Cha, B.-J. Yi, and W. K. Kim, "Implementation of a 4-dof parallel mechanism as a needle insertion device," in *Robotics and Automation (ICRA), 2010 IEEE International Conference on*, pp. 662–668, IEEE, 2010.

[11] L. Goffin, G. Bour, F. Martel, S. Nicolau, J. Gangloff, J.-M. Egly, and B. Bayle, "Design and in vivo evaluation of a robotized needle insertion system for small animals," *IEEE Transactions on Biomedical Engineering*, vol. 60, no. 8, pp. 2193–2204, 2013.

[12] J. Huang, J. K. Triedman, N. V. Vasilyev, Y. Suematsu, R. O. Cleveland, and P. E. Dupont, "Imaging artifacts of medical instruments in ultrasound-guided interventions," *Journal of Ultrasound in Medicine*, vol. 26, no. 10, pp. 1303–1322, 2007.

[13] O. Bebek, M. J. Hwang, and M. C. Cavusoglu, "Design of a parallel robot for needle-based interventions on small animals," *Mechatronics, IEEE/ASME Transactions on*, vol. 18, no. 1, pp. 62–73, 2013.

[14] Y. Moon and J. Choi, "A planar compliant parallel robotic mechanism for robotic needle intervention," in *Control, Automation and Systems (ICCAS), 2013 13th International Conference on*, pp. 92–95, IEEE, 2013.

[15] J. Morse, N. Terrasini, M. Wehbe, C. Philippona, C. Zaouter, S. Cyr, and T. Hemmerling, "Comparison of success rates, learning curves, and inter-subject performance variability of robot-assisted and manual ultrasound-guided nerve block needle guidance in simulation," *British journal of anaesthesia*, vol. 112, no. 6, pp. 1092–1097, 2014.

[16] M. S. Sabel, C. S. Kaufman, P. Whitworth, H. Chang, L. H. Stocks, R. Simmons, and M. Schultz, "Cryoablation of early-stage breast cancer: work-in-progress report of a multi-institutional trial," *Annals of surgical oncology*, vol. 11, no. 5, pp. 542–549, 2004.

[17] E. D. Staren, M. S. Sabel, L. M. Gianakakis, G. A. Wiener, V. M. Hart, M. Gorski, K. Dowlatshahi, B. F. Corning, M. F. Haklin, and G. Koukoulis, "Cryosurgery of breast cancer," *Archives of Surgery*, vol. 132, no. 1, pp. 28–33, 1997.

[18] S. O. Pfleiderer, M. G. Freesmeyer, C. Marx, R. Kühne-Heid, A. Schneider, and W. A. Kaiser, "Cryotherapy of breast cancer under ultrasound guidance: initial results and limitations," *European radiology*, vol. 12, no. 12, pp. 3009–3014, 2002.

[19] J. Kettenbach, G. Kronreif, M. Figl, M. Fürst, W. Birkfellner, R. Hanel, and H. Bergmann, "Robot-assisted biopsy using ultrasound guidance: initial results from in vitro tests," *European radiology*, vol. 15, no. 4, pp. 765–771, 2005.

[20] M. Kaya and O. Bebek, "Needle localization using gabor filtering in 2d ultrasound images," in *Robotics and Automation (ICRA), 2014 IEEE International Conference on*, pp. 4881–4886, IEEE, 2014.

[21] M. Kaya and O. Bebek, "Gabor filter based localization of needles in ultrasound guided robotic interventions," in *Imaging Systems and Techniques (IST), 2014 IEEE International Conference on*, pp. 112–117, IEEE, 2014.

[22] S. O. Orhan, M. C. Yildirim, and O. Bebek, "Design and modeling of a parallel robot for ultrasound guided percutaneous needle interventions," in *Industrial Electronics Society, IECON 2015-41st Annual Conference of the IEEE*, pp. 005002–005007, IEEE, 2015.

[23] M. Kaya, E. Senel, A. Ahmad, O. Orhan, and O. Bebek, "Real-time needle tip localization in 2d ultrasound images for robotic biopsies," *17th International Conference on Advanced Robotics*, 2015.

[24] M. Kaya, E. Senel, A. Ahmad, O. Orhan, and O. Bebek, "Real-time needle tip localization in 2d ultrasound images for robotic biopsies," in *Advanced Robotics (ICAR), 2015 International Conference on*, pp. 47–52, IEEE, 2015.

[25] A. Ahmad, M. C. Cavusoglu, and O. Bebek, "Calibration of 2d ultrasound in 3d space for robotic biopsies," in *Advanced Robotics (ICAR), 2015 International Conference on*, pp. 40–46, IEEE, 2015.

[26] L. F. Smith, I. T. Rubio, R. Henry-Tillman, S. Korourian, and V. S. Klimberg, "Intraoperative ultrasound-guided breast biopsy," *The american journal of surgery*, vol. 180, no. 6, pp. 419–423, 2000.

[27] M. D. Rifkin, F. E. Rosato, H. M. Branch, J. Foster, S. Yang, D. J. Barbot, and G. J. Marks, "Intraoperative ultrasound of the liver. an important adjunctive tool for decision making in the operating room.," *Annals of surgery*, vol. 205, no. 5, p. 466, 1987.

[28] H. Neshat, D. W. Cool, K. Barker, L. Gardi, N. Kakani, and A. Fenster, "A 3d ultrasound scanning system for image guided liver interventions," *Medical physics*, vol. 40, no. 11, p. 112903, 2013.

[29] T. R. Nelson and D. H. Pretorius, "Three-dimensional ultrasound imaging," *Ultrasound in medicine & biology*, vol. 24, no. 9, pp. 1243–1270, 1998.

[30] A. M. Priester, S. Natarajan, and M. O. Culjat, "Robotic ultrasound systems in medicine," *IEEE transactions on ultrasonics, ferroelectrics, and frequency control*, vol. 60, no. 3, pp. 507–523, 2013.

[31] L. Mercier, T. Langø, F. Lindseth, and L. D. Collins, "A review of calibration techniques for freehand 3-d ultrasound systems," *Ultrasound in medicine & biology*, vol. 31, no. 2, pp. 143–165, 2005.

[32] S. Tong, D. Downey, H. Cardinal, and A. Fenster, "A three-dimensional ultrasound prostate imaging system," *Ultrasound in medicine & biology*, vol. 22, no. 6, pp. 735–746, 1996.

[33] P.-C. Li, C.-Y. Li, and W.-C. Yeh, "Tissue motion and elevational speckle decorrelation in freehand 3d ultrasound," *Ultrasonic imaging*, vol. 24, no. 1, pp. 1–12, 2002.

[34] L. E. Bø, E. F. Hofstad, F. Lindseth, and T. A. Hernes, "Versatile robotic probe calibration for position tracking in ultrasound imaging," *Physics in medicine and biology*, vol. 60, no. 9, p. 3499, 2015.

[35] Y. Sato, M. Nakamoto, Y. Tamaki, T. Sasama, I. Sakita, Y. Nakajima, M. Monden, and S. Tamura, "Image guidance of breast cancer surgery using 3-d ultrasound images and augmented reality visualization," *Medical Imaging, IEEE Transactions on*, vol. 17, no. 5, pp. 681–693, 1998.

[36] H. Zhang, F. Banovac, A. White, and K. Cleary, "Freehand 3d ultrasound calibration using an electromagnetically tracked needle," in *Medical Imaging*, pp. 61412M–61412M, International Society for Optics and Photonics, 2006.

[37] R. W. Prager, R. Rohling, A. Gee, and L. Berman, "Rapid calibration for 3-d freehand ultrasound," *Ultrasound in medicine & biology*, vol. 24, no. 6, pp. 855–869, 1998.

[38] E. M. Boctor, A. Jain, M. A. Choti, R. H. Taylor, and G. Fichtinger, "Rapid calibration method for registration and 3d tracking of ultrasound images using spatial localizer," in *Medical Imaging 2003*, pp. 521–532, International Society for Optics and Photonics, 2003.

[39] J. M. Blackall, D. Rueckert, C. R. Maurer Jr, G. P. Penney, D. L. Hill, and D. J. Hawkes, "An image registration approach to automated calibration for freehand 3d ultrasound," in *Medical Image Computing and Computer-Assisted Intervention–MICCAI 2000*, pp. 462–471, Springer, 2000.

[40] T. Chen, P. Abolmaesumi, A. Thurston, and R. Ellis, "Automated 3d freehand ultrasound calibration with real-time accuracy control," *Medical Image Computing and Computer-Assisted Intervention–MICCAI 2006*, pp. 899–906, 2006.

[41] Euresys, "Picolo hd 3g frame grabber." `http://www.euresys.com/product/picolo-hd-3g/?tabproduct=benefits`.

[42] OptiTrack, "Motive." `http://optitrack.com/products/motive/`.

[43] J. Huang, J. K. Triedman, N. V. Vasilyev, Y. Suematsu, R. O. Cleveland, and P. E. Dupont, "Imaging artifacts of medical instruments in ultrasound-guided interventions," *Journal of Ultrasound in Medicine*, vol. 26, no. 10, pp. 1303–1322, 2007.

[44] S. DiMaio, S. Pieper, K. Chinzei, N. Hata, S. Haker, D. Kacher, G. Fichtinger, C. Tempany, and R. Kikinis, "Robot-assisted needle placement in open mri: system architecture, integration and validation," *Computer Aided Surgery*, vol. 12, no. 1, pp. 15–24, 2007.

[45] E. Coste-Maniere and R. Simmons, "Architecture, the backbone of robotic systems," in *Robotics and Automation, 2000. Proceedings. ICRA'00. IEEE International Conference on*, vol. 1, pp. 67–72, IEEE, 2000.

[46] J. S. Albus, R. Lumia, and H. McCain, "Hierarchical control of intelligent machines applied to space station telerobots," *IEEE transactions on aerospace and electronic systems*, vol. 24, no. 5, pp. 535–541, 1988.

[47] R. Brooks, "A robust layered control system for a mobile robot," *IEEE journal on robotics and automation*, vol. 2, no. 1, pp. 14–23, 1986.

[48] D. J. Musliner, E. H. Durfee, and K. G. Shin, "Circa: A cooperative intelligent real-time control architecture," *IEEE Transactions on Systems, Man, and Cybernetics*, vol. 23, no. 6, pp. 1561–1574, 1993.

[49] J. Bellingham and J. Leonard, "Task configuration with layered control," in *IARP 2nd workshop on mobile robots for subsea environments*, 1994.

[50] G. Moustris, S. Hiridis, K. Deliparaschos, and K. Konstantinidis, "Evolution of autonomous and semi-autonomous robotic surgical systems: a review of the literature," *The International Journal of Medical Robotics and Computer Assisted Surgery*, vol. 7, no. 4, pp. 375–392, 2011.

[51] V. G. Mallapragada, N. Sarkar, and T. K. Podder, "Robot-assisted real-time tumor manipulation for breast biopsy," *IEEE Transactions on Robotics*, vol. 25, no. 2, pp. 316–324, 2009.

[52] K. Sharma, W. S. Newman, M. Weinhous, G. Glosser, and R. Macklis, "Experimental evaluation of a robotic image-directed radiation therapy system," in *Robotics and Automation, 2000. Proceedings. ICRA'00. IEEE International Conference on*, vol. 3, pp. 2913–2918, IEEE, 2000.

[53] A. Schweikard, G. Glosser, M. Bodduluri, M. J. Murphy, and J. R. Adler, "Robotic motion compensation for respiratory movement during radiosurgery," *Computer Aided Surgery*, vol. 5, no. 4, pp. 263–277, 2000.

[54] C. Riviere, A. Thakral, I. Iordachita, G. Mitroi, and D. Stoianovici, "Predicting respiratory motion for active canceling during percutaneous needle insertion," in *Engineering in Medicine and Biology Society, 2001. Proceedings of the 23rd Annual International Conference of the IEEE*, vol. 4, pp. 3477–3480, IEEE, 2001.

[55] A. L. Trejos, S. Salcudean, F. Sassani, and S. Lichtenstein, "On the feasibility of a moving support for surgery on the beating heart," in *International Conference on Medical Image Computing and Computer-Assisted Intervention*, pp. 1088–1097, Springer, 1999.

[56] B. D. Anderson and J. B. Moore, *Linear optimal control*. Prentice-Hall Englewood Cliffs, 1971.

[57] W. H. Kwon and S. H. Han, *Receding horizon control: model predictive control for state models*. Springer Science & Business Media, 2006.

[58] E. F. Camacho and C. B. Alba, *Model predictive control*. Springer Science & Business Media, 2013.

[59] O. Bebek, *Robotic-assisted beating heart surgery*. PhD thesis, Case Western Reserve University, 2008.

[60] S. R. Mousavi, K. Raahemifar, S. Pautler, and A. Samani, "Towards ultrasound probe positioning optimization during prostate needle biopsy using pressure feedback," *International journal of computer assisted radiology and surgery*, vol. 8, no. 6, pp. 1053–1061, 2013.

# VITA

Mr. Awais Ahmad completed his Bachelor's in Mechatronics and Control Engineering from University of Engineering and Technology, Lahore, Pakistan in 2013. After graduating, Mr. Ahmad joined Al'Khawarizmi Institute of Computer Science (KICS), where his research area was Near Field Communication (NFC) Technology. While working there, he worked on developing smart phone and stand-alone applications of NFC for Private and Public sector. Mr. Ahmad joined Ozyegin University Robotics Lab in 2014 and started to work with Dr. Ozkan Bebek.